DOW CHEMICAL COMPANY
RESEARCH REACTOR
LICENSE NO. R-108
DOCKET NO. 50-264

TECHNICAL RAI RESPONSES (DATED 12/06/2011)

REDACTED VERSION*

SECURITY-RELATED INFORMATION REMOVED

*REDACTED TEXT AND FIGURES BLACKED OUT OR DENOTED BY BRACKETS

The Dow Chemical Company
Midland, Michigan 48667

[redacted]

Mr. Geoffrey Wertz
Research and Test Reactors Licensing Branch
Division of Policy and Rulemaking
Office of Nuclear Reactor Regulation

Subject: The Dow Chemical Company- License No. R-108; Docket No. 50-264

Enclosed are the updated Neutronic and Thermal Hydraulic reports in support of the DTRR license renewal. The DTRR is hereby withdrawing Neutronic and Thermal Hydraulic reports dated October 11, and October 8, 2011 respectively, previously submitted on November 10, 2011, and replacing them with these updated reports dated December 3, 2011.

Should you have any questions or need additional information, please contact the Facility Director, Paul O'Connor, at 989-638-6185.

I declare under penalty of perjury that the foregoing is true and correct.

Executed on December 06, 2011

Paul O'Connor

Paul O'Connor, Ph.D.
Director
Dow TRIGA Research Reactor

Subscribed and sworn to before me this 6th day of December, 2011

Jennifer Lyn Obertein
Notary Public
Saginaw County, Michigan
My Commission Expires:
June 22, 2012

Jennifer Lyn Obertein
NOTARY PUBLIC, SAGINAW COUNTY, MICHIGAN
MY COMMISSION EXPIRES JUNE 22, 2012
ACTING IN THE COUNTY OF Midland

cc: Wayde Konze, R&D Director - Analytical Sciences
Paul O'Connor, Director
Siaka Yusuf, Reactor Supervisor

A020
NRR

ANALYSIS OF THE THERMAL HYDRAULIC AND REACTIVITY INSERTION BEHAVIOR OF THE DOW TRIGA RESEARCH REACTOR

Submitted to the NRC in support of the DTRR License Renewal

Prepared by:

Michael R Hartman

03 December 2011

TABLE OF CONTENTS

LIST OF TABLES

LIST OF FIGURES

1. Introduction

The following report summarizes an investigation into the thermal hydraulic behavior and the response to reactivity insertions of the DOW TRIGA Research Reactor (DTRR). The DTRR is a TRIGA Mark-I reactor which is licensed to operate at powers up to 300 kW. The reactor consists of a series of six concentric rings in which are located fuel elements, graphite reflectors, and various experimental facilities. The core is surrounded by a cylindrical annulus of graphite which acts as a neutron reflector. The core and reflector are located in a below-grade aluminum tank filled with high-purity water. The water acts as a neutron moderator, a coolant, and as a radiation shield. Heat produced within the DTRR is rejected from the fuel to the water in the tank via natural convection cooling.

The purpose of this report is to provide a modern analysis of the thermal hydraulic characteristics of the DTRR in support of a 20-year license renewal through the U.S. Nuclear Regulatory Commission. Thermal hydraulic modeling of the DTRR was done using RELAP5-3D.[1] The reactivity accidents were analyzed using a point-kinetics model of the DTRR in conjunction with data from the recent neutronic and thermal hydraulic analyses of the DTRR. The results of these analyses provide a basis to evaluate the thermal hydraulic and reactivity accident performance of the DTRR in support of the license renewal.

2. Thermal Hydraulic Analysis

To analyze the thermal hydraulic performance of the DTRR a "hot-channel" methodology was employed whereby the most limiting thermal hydraulic channel in the DTRR is coupled to the fuel element with the highest power production. It should be noted that in reality the highest power element is not necessarily associated with the most limiting thermal hydraulic channel. However, performing the analysis in this manner creates a bounding analysis for all possible combinations of hot rods and thermal hydraulic channels in the DTRR. The limiting thermal hydraulic channel in the DTRR exists in the B-ring where the fuel elements have a hexagonal arrangement with an element-to-element pitch, P, of 0.04054 m. The limiting thermal hydraulic channel in the DTRR is shown schematically in Figure 1. The outer diameter of the fuel elements, D_{Fuel}, for the DTRR fuel is 0.03747 m. Using these, the flow area of the limiting thermal hydraulic channel was found, using Equation (1),

$$A_{Flow} = \frac{\sqrt{3}}{2}P^2 - \frac{\pi}{4}D_{Fuel}^2, \quad (1)$$

to be 3.21E-4 m^2. The hydraulic diameter, D_h, is calculated using Equation (2),

$$D_h = \frac{4(A_{Flow})}{(Wetted\ perimeter)}, \quad (2)$$

1. RELAP5-3D Code Development Team, "Volume 1: code structure, system models, and solution methods, in RELAP5-3D code manual" Idaho National Laboratory, Idaho Falls, ID (2005).

resulting in a hydraulic diameter of 1.09E-2 m for the limiting thermal hydraulic channel in the DTRR.

Using this data, a model of the hot-channel was constructed in RELAP5-3D. The model conservatively assumes that there is no cross flow amongst adjacent thermal hydraulic channels. In reality, there will be mixing between adjacent thermal hydraulic channels and as such the analysis reported herein has an inherent level of conservatism. The geometry and loss coefficients utilized within the RELAP5-3D model are summarized in Table 1 and Table 2, respectively.

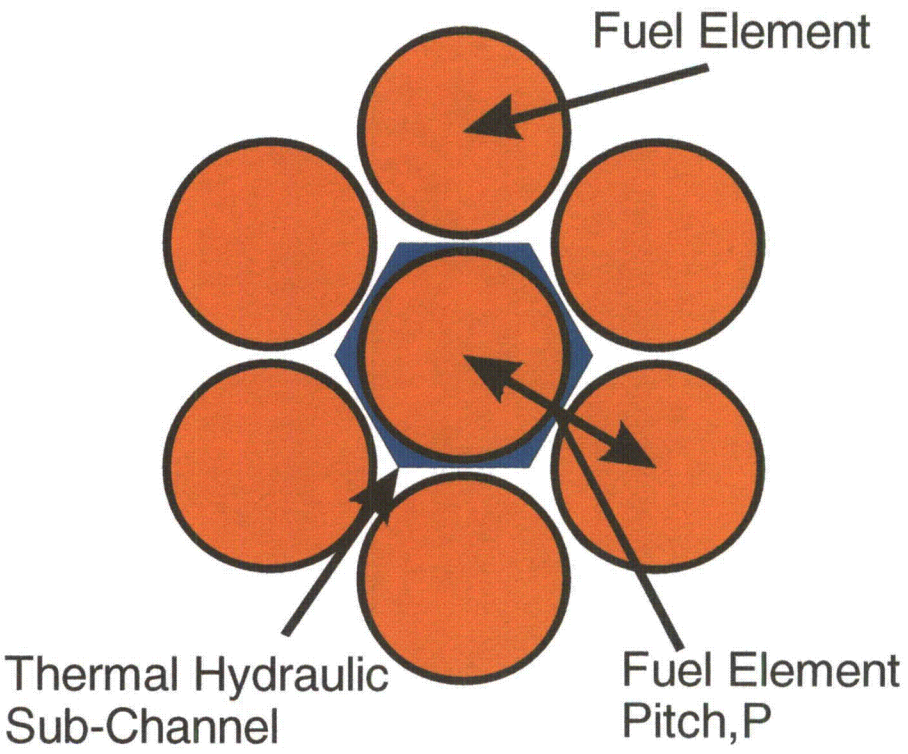

Figure 1. Schematic illustration of the thermal hydraulic sub-channel utilized in the analysis of the thermal hydraulic performance of the DTRR.

Table 1. Physical data utilized in the RELAP5-3D model of the DTRR.

Parameter	Value
Flow area [m^2]	3.21E-04
Fuel Element Pitch [m]	4.05E-02
Wetted Perimeter [m]	1.18E-01
Hydraulic diameter [m]	1.09E-02
Diameter of heated region [m]	[redacted]
Fuel element heated length [m]	[redacted]
Fuel element surface area [m^2]	[redacted]
Fuel element surface roughness [m]	2.13E-06

Table 2. Loss coefficients utilized in the RELAP5-3D model of the DTRR.

Description	Coefficient
Inlet pressure loss coefficient	2.26
Exit pressure loss coefficient	0.63

The RELAP5-3D model used to analyze the thermal hydraulic performance of the DTRR is shown schematically in Figure 2. The model consists of a coolant source (volume 100), a cold leg (volume 101), a horizontal connector (volume 102), a hot channel (volume 103), and a coolant sink (volume 104). The coolant source permits the application of the time-dependent pressure and temperature boundary conditions for the thermal hydraulic analysis. The cold leg is used to establish the pressure differential across the thermal hydraulic sub channel and is utilized to establish the natural convection flow through the channel. The horizontal connector only serves to provide a physical connection between the cold leg and the hot channel. The hot channel contains the fuel element with the highest power and the limiting thermal hydraulic channel (corresponding in this case to the thermal hydraulic channels in the B-ring). The fuel element volume within the RELAP5-3D model is discretized both axially and radially, as shown in Figures 3 and 4. The discretization corresponds to that applied within the neutronics calculation and permits the power densities determined in the neutronics calculations to be directly applied to the heat source within the RELAP5-3D hot channel model. For the axial discretization, the upper and lower grid plates (nodes 01 and 24) have a length of 0.01905 m, the lower graphite region (node 02) has a length of 0.14643 m, the nodes in the fueled region (nodes 03 through 22) have a length of 0.01905 m, and the upper graphite region (node 23) has a length of 0.14567 m. For the radial discretization, node 01 is located on the centerline of the fuel, the zirconium pin (node 02) has a radius of 0.00318 m, each of the fuel nodes (nodes 03 to 22) are separated by a radial distance of 0.0007335 m, the outer gap has a thickness of 1E-05 m, and the cladding thickness is 0.00087 m. The gap thickness of 1E-05 m is consistent with the expected gap in the fuel elements after at-power operation as a result of swelling of the fuel slugs and the concomitant closing of the as-manufactured gap when the elements are assembled during manufacture.

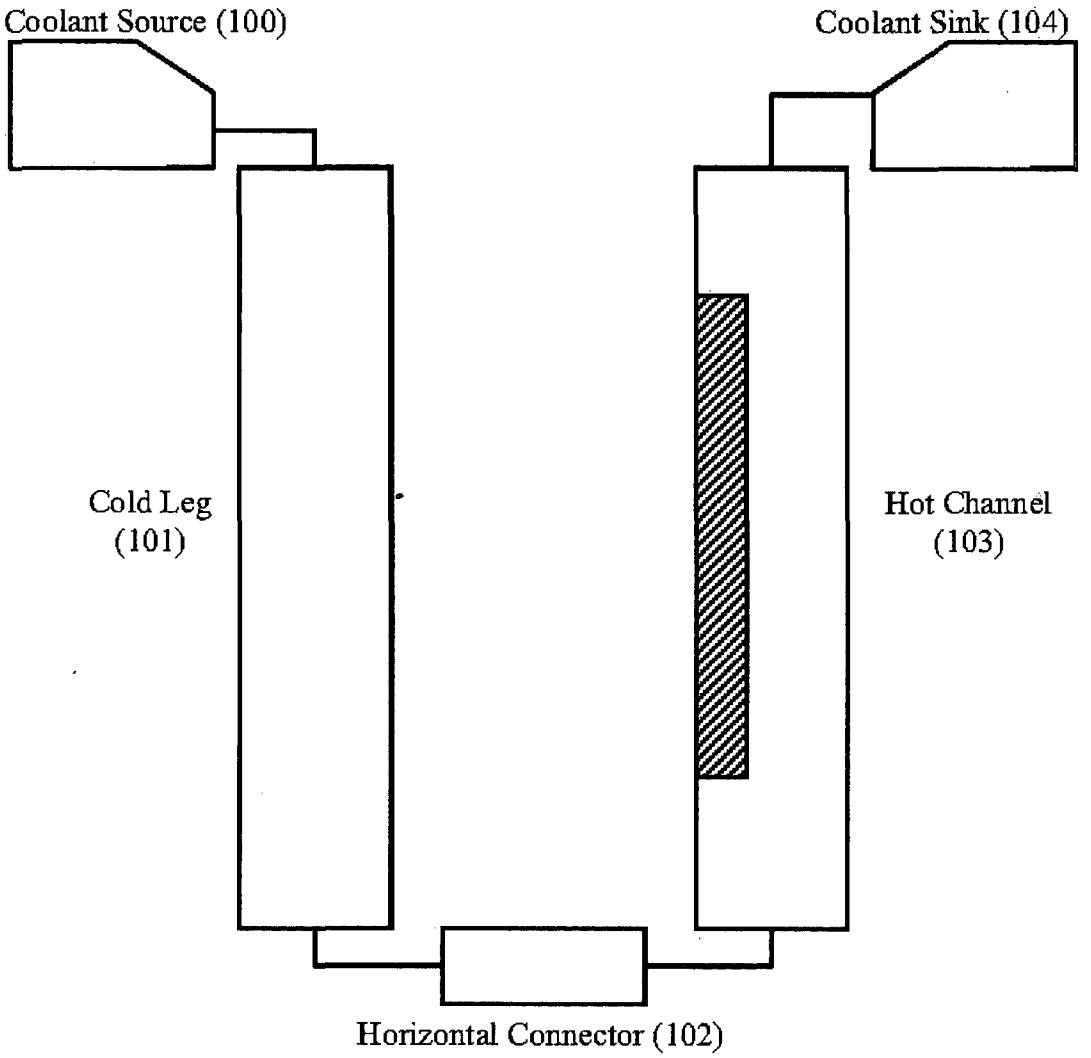

Figure 2. Schematic illustration of the RELAP5-3D hot channel model utilized in the thermal hydraulic analysis of the DTRR.

Figure 3. A schematic illustration of the profile of a DTRR fuel element (right) along with a cross sectional view, showing the internal structure of the fuel element (left). The axial discretization used to establish the nodes in the RELAP5-3D model are shown adjacent to the cross sectional view.

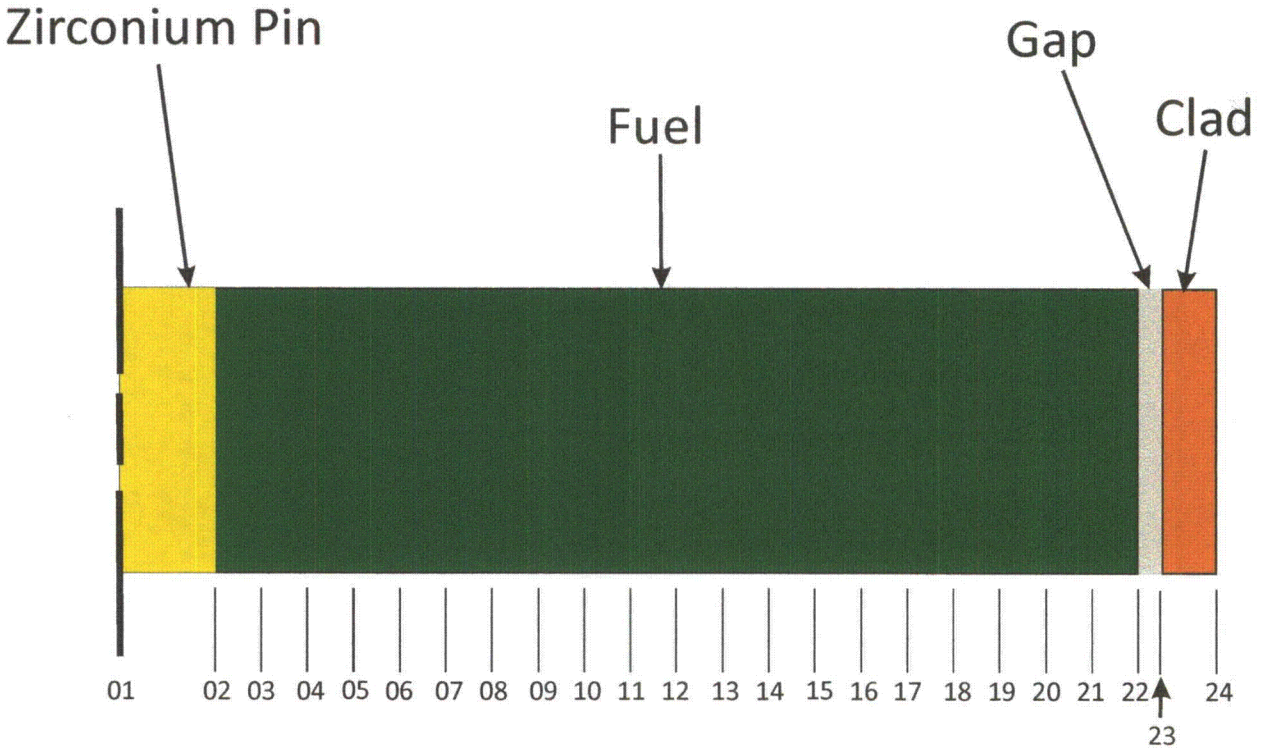

Figure 4. Schematic illustration of the radial discretization utilized within the RELAP5-3D model of the DTRR. The nodes are show below the radial cross section

The Bernath correlation[2] was used in the analysis of the thermal hydraulic performance of the DTRR. The choice of Bernath was predicated on the following factors: 1) the correlation has been extensively used for the analysis of research reactors, and 2) the DNBR predictions from the Bernath correlation have been shown to be conservative with respect to other potential choices for the correlation.

Three separate cases were considered for the thermal hydraulic analysis of the DTRR. Case #1 corresponds to the nominal operating characteristics of the DTRR for the 2011 core configuration with a reactor power level of 300 kW, a bulk pool temperature of 25 °C, and a pool level of 16 feet above the top of the core. Case #2 again utilizes the 2011 core configuration, but this time assumes the limiting thermal hydraulic conditions with a power level of 300 kW, a pool inlet temperature of 60 °C, and a pool level of 15 feet above the top of the core. Case #3 is based upon the limiting core configuration (LCC) which was analyzed in the neutronics analysis of the DTRR. This core represents extreme power peaking in the DTRR due to possible reconfiguration of the DTRR core. The LCC core configuration was used in conjunction with a reactor power level of 300 kW, a pool inlet temperature of 60 °C, and a pool level of 15 feet

2. Bernath, L., "A Theory of Local Boiling Burnout and Its Application to Existing Data," Heat Transfer – Chemical Engineering Progress Symposium Series No. 30, 56, pp95-116 (1960).

above the top of the core. The three cases are summarized in Table 3 below, where the hot rod power was as determined in the detailed neutronics analysis of the DTRR, the details of which are provided in a separate report.

Table 3. Summary of conditions for the three thermal hydraulic cases considered in the analysis of the thermal hydraulic performance of the DTRR.

	Case #1	Case #2	Case #3
Hot Rod Power [kW]	5.91	5.91	6.08
Pool Inlet Temperature [°C]	25	60	60
Pool Level Above DTRR Core [ft]	16	15	15

For the 2011 core configuration, the normalized axial and radial power profiles for the hot rod are shown in Figures 5 and 6, respectively. While for the LCC, the normalized axial and radial power profiles are shown in Figures 7 and 8, respectively.

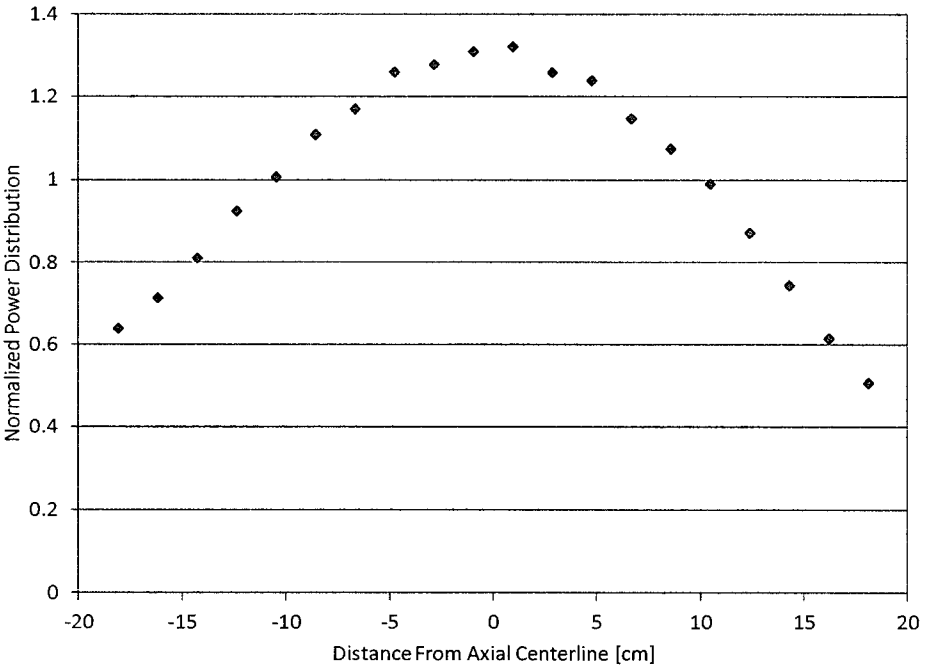

Figure 5. Normalized axial power profile for the hot rod (element B-6) in the 2011 core configuration of the DTRR.

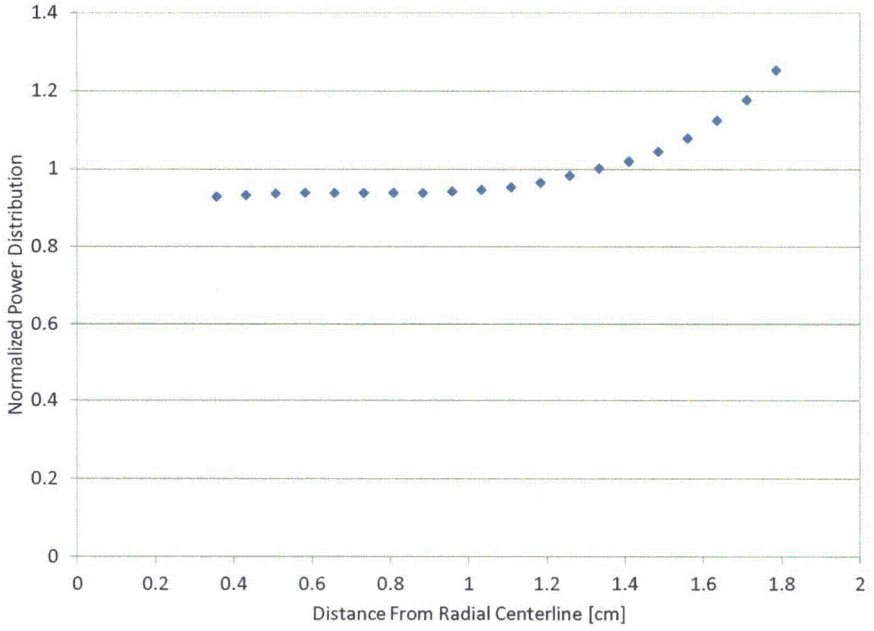

Figure 6. Normalized radial power profile for the hot rod (element B-6) in the 2011 core configuration of the DTRR

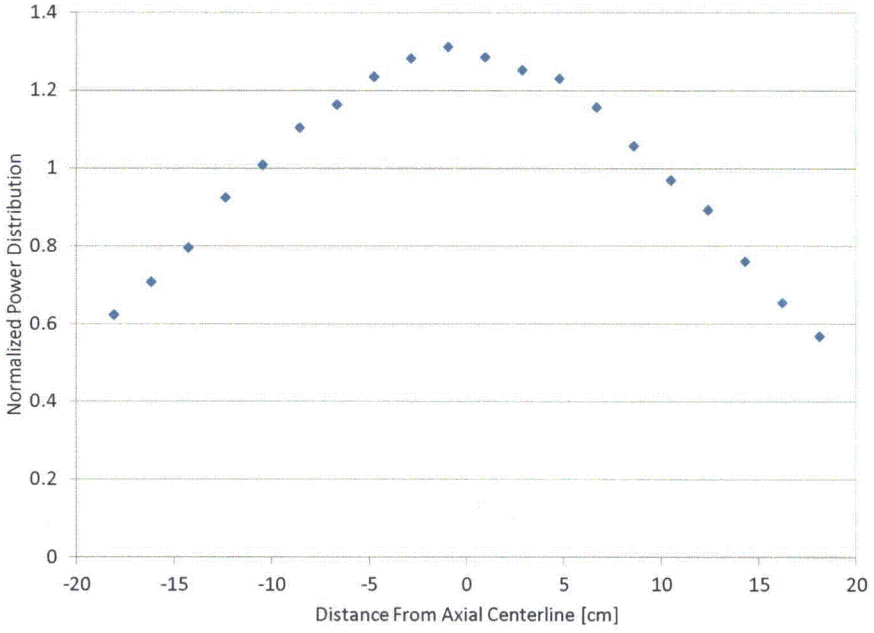

Figure 7. Normalized axial power profile for the hot rod (element C-6) in the LCC core configuration of the DTRR.

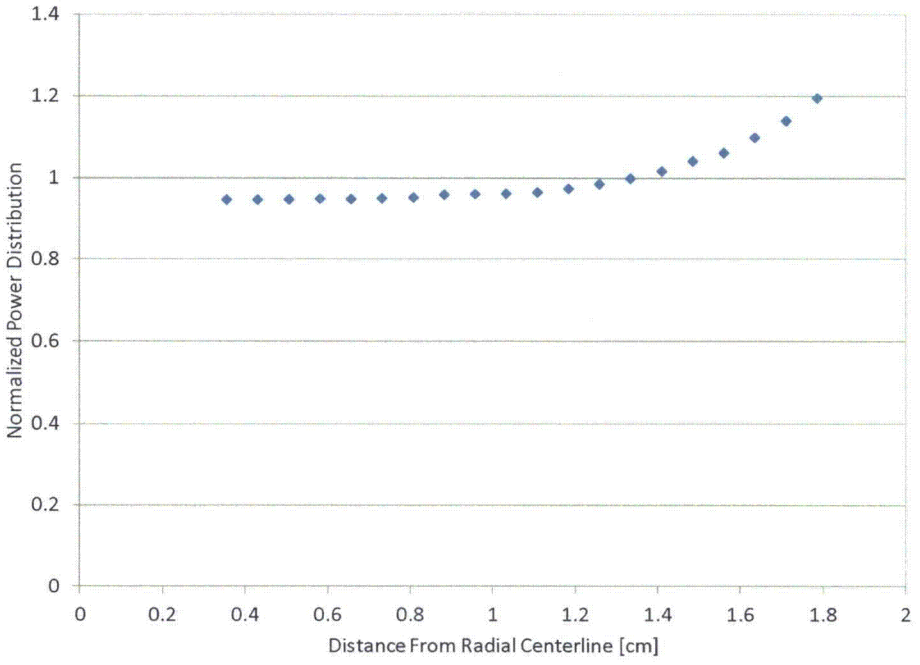

Figure 8. Normalized axial power profile for the hot rod (element C-6) in the LCC core configuration of the DTRR.

For Case #1, the axial profile for the fuel centerline temperature, the clad outer temperature, and the bulk coolant are shown in Figure 9. The results of the analysis are summarized in Table 4, where it can be seen that the DNBR predicted by the Bernath correlation is 9.99.

Table 4. Summary of thermal hydraulic analysis for Case #1.

Parameter Description	Value
Rod Power [kW]	5.91
Hot Channel Fuel Element Peaking Factor $[P_{max}/P_{avg}]_{Element}$	1.576
Hot Channel Fuel Axial Peaking Factor $[P_{max}/P_{avg}]_{Axial\ nodes}$	1.322
Hot Channel Fuel Radial Peaking Factor $[P_{max}/P_{avg}]_{Radial\ nodes}$	1.254
Maximum Fuel Temperature [°C]	240.30
Maximum Outer Cladding Temperature [°C]	121.06
Minimum Predicted DNBR (Bernath Correlation)	9.99

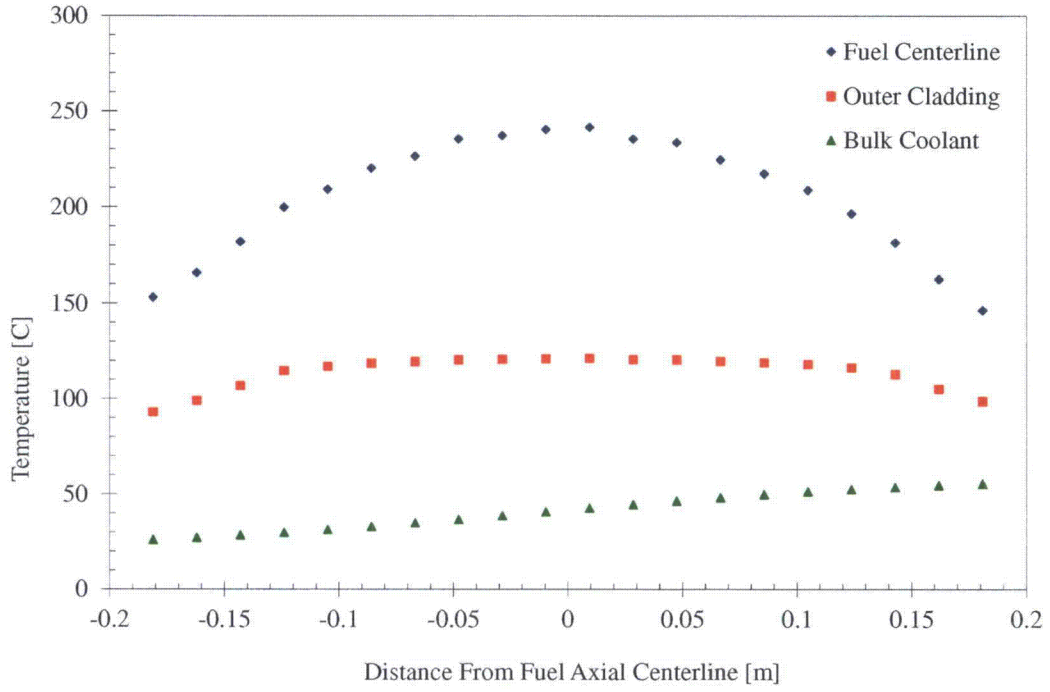

Figure 9. Fuel centerline, outer cladding, and bulk coolant temperature for the hot-channel in Case #1.

For Case #2, the axial profile for the fuel centerline temperature, the clad outer temperature, and the bulk coolant are shown in Figure 10. The results of the analysis are summarized in Table 5, where it can be seen that the minimum DNBR predicted by the Bernath correlation is 6.81.

Table 5. Summary of thermal hydraulic analysis for Case #2.

Parameter Description	Value
Rod Power [kW]	5.91
Hot Channel Fuel Element Peaking Factor $[P_{max}/P_{avg}]_{Element}$	1.576
Hot Channel Fuel Axial Peaking Factor $[P_{max}/P_{avg}]_{Axial\ nodes}$	1.322
Hot Channel Fuel Radial Peaking Factor $[P_{max}/P_{avg}]_{Radial\ nodes}$	1.254
Maximum Fuel Temperature [°C]	241.69
Maximum Outer Cladding Temperature [°C]	122.56
Minimum Predicted DNBR (Bernath Correlation)	6.81

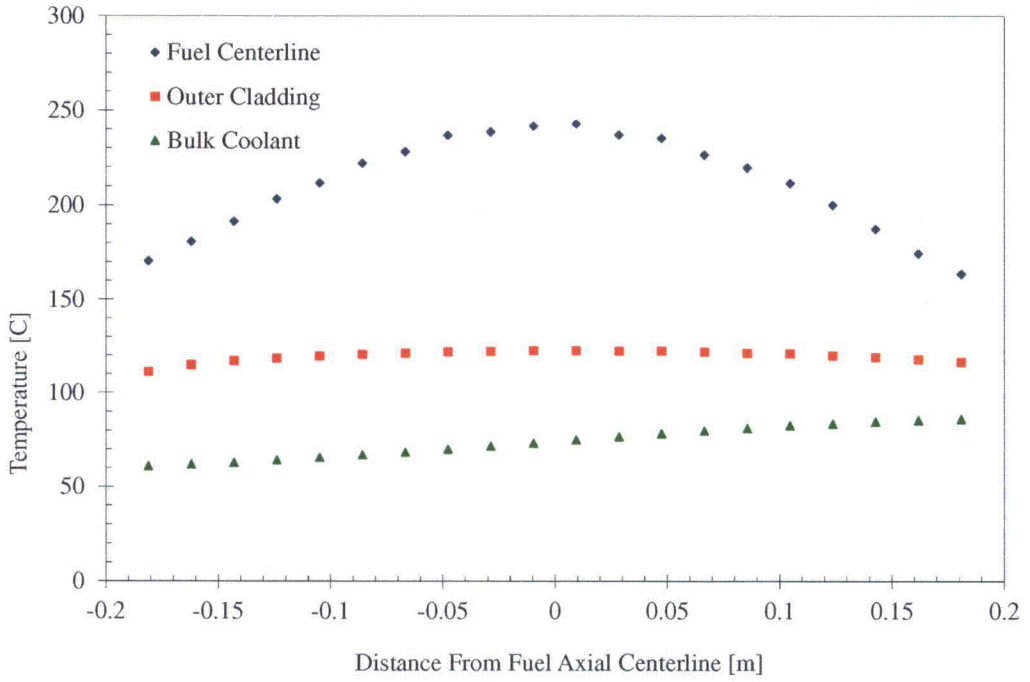

Figure 10. Fuel centerline, outer cladding, and bulk coolant temperature for the hot-channel in Case #2.

For Case #3, the axial profile for the fuel centerline temperature, the clad outer temperature, and the bulk coolant are shown in Figure 11. The results of the analysis are summarized in Table 6, where it can be seen that the minimum DNBR predicted by the Bernath correlation is 6.76.

Table 6. Summary of thermal hydraulic analysis for Case #3.

Parameter Description	Value
Rod Power [kW]	6.08
Hot Channel Fuel Element Peaking Factor $[P_{max}/P_{avg}]_{Element}$	1.539
Hot Channel Fuel Axial Peaking Factor $[P_{max}/P_{avg}]_{Axial\ nodes}$	1.312
Hot Channel Fuel Radial Peaking Factor $[P_{max}/P_{avg}]_{Radial\ nodes}$	1.196
Maximum Fuel Temperature [°C]	246.70
Maximum Outer Cladding Temperature [°C]	122.84
Minimum Predicted DNBR (Bernath Correlation)	6.76

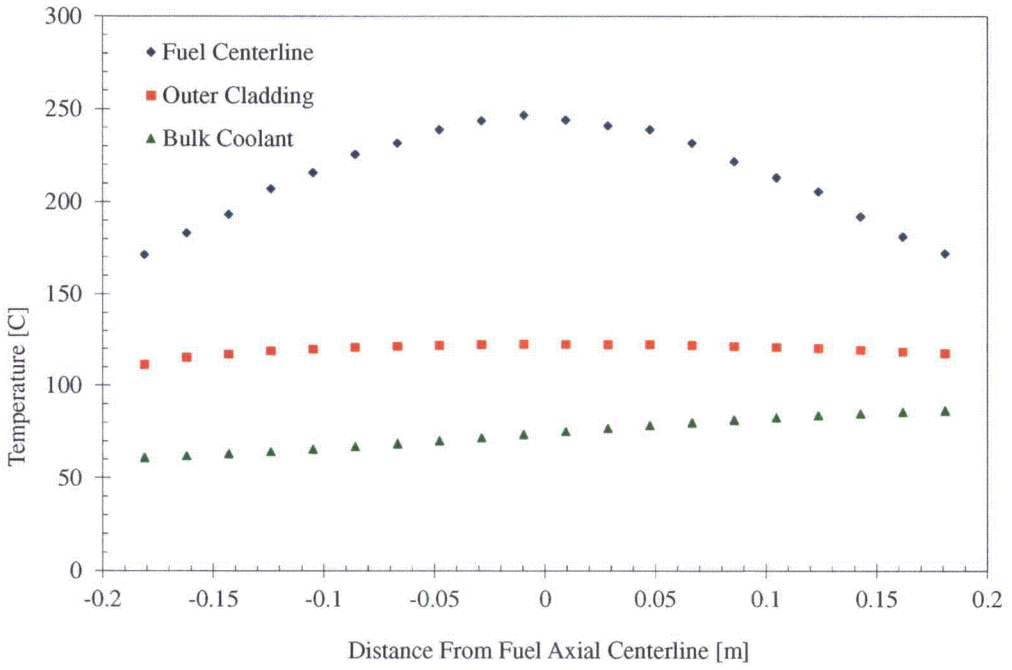

Figure 11. Fuel centerline, outer cladding, and bulk coolant temperature for the hot-channel in Case #3.

Note that in all cases, the minimum DNBR predicted by the Bernath correlation is well above the limiting minimum DNBR of 2.0 which is typically applied to research reactors.

3. Reactivity Insertions

To verify the validity of the DTRR Safety Limit which states that *"The temperature in any fuel element in the DOW TRIGA Research Reactor shall not exceed 500 °C under any condition of operation."*, calculations were performed to assess the response of the DTRR to postulated reactivity insertion events. Two such events were considered. The first of these was a step insertion of reactivity corresponding to the maximum worth of a moveable experiment in the DTRR ($0.75, DTRR Technical Specification 3.7.3). The second reactivity insertion considered was the uncontrolled withdrawal of a control rod at the maximum allowed reactivity insertion rate ($0.20/s, DTRR SAR Table 4). In each case a point-kinetics model was developed and solved numerically to determine the peak fuel temperature observed in response to the event. The point-kinetics model is as follows:

$$\frac{dP(t)}{dt} = \left[\frac{\rho(t) - \bar{\beta}}{\Lambda}\right] P(t) + \sum_{i=1}^{6} \lambda_i C_i(t) + S(t); \qquad i = 1, \ldots, 6$$

$$\frac{dC_i(t)}{dt} = \frac{\bar{\beta}_i}{\Lambda} P(t) - \lambda_i C_i(t)$$

$$\rho(t) = \rho_{Reactivity\ event}(t) + \rho_{Feedback}(t)$$

$$\Lambda = \frac{l}{k(t)}$$

$$k(t) = \frac{1}{1-\rho(t)}$$

$$\rho_{Feedback}(t) = \alpha_{Fuel}(T_{Fuel}(t) - T_{Fuel}(0))$$

and

$$\frac{dT_{Fuel}(t)}{dt} = \frac{[P(t) - P(0)]}{m_{Fuel}C_{P_{Fuel}}(T)}$$

where $\rho(t)$ is the reactivity at time t, $\bar{\beta}$ is the effective delayed neutron fraction, l is the prompt-neutron lifetime, Λ is the mean generation time, λ_i is the decay constant for the i^{th} delayed neutron precursor group, $C_i(t)$ is the density of delayed neutron precursors in the i^{th} group, S(t) is an external source, k(t) is the time-dependent multiplication factor, $T_{Fuel}(t)$ is the average core fuel temperature, m_{Fuel} is the mass of the fuel, and $C_P(T)$ is the specific heat capacity of the fuel. For the calculations performed herein, the following additional assumptions were made:

1. External sources, S(t), can be ignored
2. The mean generation time, Λ, was taken to be the same as the prompt-neutron lifetime, l.
3. The fuel elements were treated adiabatically (i.e. no heat rejection to the coolant) resulting in conservative estimates of the fuel temperature in response to a reactivity event.
4. The product $m_{Fuel}C_{P\_Fuel}$ was taken to be $825 + 1.61*(T_{Fuel}-25)$ W·sec/(°C·fuel element), where T_{Fuel} is in units of °C.[3]

The step insertion of the maximum worth of a moveable experiment ($0.75) was analyzed first. The initial fuel temperature, $T_{Fuel}(0)$, was taken to be 200°C, a value of 0.0070 for $\bar{\beta}$ was used, the prompt-neutron lifetime was taken to be 60 μsec, and a value of -$0.0181/°C was used for the fuel temperature reactivity coefficient, α_{Fuel}. For an initial power of 300 kW, the maximum observed average fuel temperature was 255 °C, corresponding to a temperature increase of 55 °C. Based on the results presented in Section 2 of this report, the maximum peaking factor

3. M. T. Simnad, F. C. Foushee, and G. B. West, "Fuel Elements for Pulsed TRIGA Research Reactors," *Nuclear Technology* 28 (1976) 31-56.

for the highest power fuel element was 2.613 for the 2011 core configuration (as determined by taking the product of the three peaking factors stated in Tables 4 or 5). Using this, the calculated temperature rise at the hottest point in the highest power fuel element would be 2.613 * 55 °C = 143.7 °C. Adding this to the maximum fuel temperature of 246.7 °C observed for any of the three thermal hydraulic conditions considered in Section 2, the maximum predicted fuel temperature for the step removal of an experiment with the maximum moveable reactivity worth of $0.75 is found to be 390.4 °C. It should be noted that use of the highest fuel temperature (thermal hydraulic Case #3) in conjunction with the peaking factor for thermal hydraulic Cases #1 and #2 is conservative since the peaking factor for Case #3 is lower than for the other cases (2.415 versus 2.613). It should also be noted that there is >100 °C margin between the predicted maximum fuel temperature in response to this reactivity insertion and the DTRR fuel temperature Safety Limit of 500 °C. Initiation of this event from lower power levels results in correspondingly lower peak fuel temperatures and is not considered further in this report.

The uncontrolled withdrawal of a control rod at the DTRR maximum reactivity insertion rate of $0.20/s was considered next. **(NOTE:** In the recent MCNP5 neutronics calculations of the DTRR, the most reactive rod was found to be SHIM 1 with an integral rod worth of $3.65. During the most recent rod calibrations at the DTRR, the rod withdrawal times were measured, and the fastest rod withdrawal time was measured to be 41.53 seconds, corresponding to a rod speed of 21.67 inches/minute. Using a conservatively faster rod speed of 22 inches/minute and the MCNP5 calculated differential rod worth curve for SHIM 1, the maximum reactivity insertion rate for the 2011 DTTR core configuration was found to be $0.14/s which is well below the Technical Specification maximum reactivity insertion rate of $0.20/s which is used in the present analysis.**)** It was further assumed that upon insertion of the remaining two control rods that the core would be subcritical by the minimum shutdown margin of $0.50. The limiting transient was determined to occur for low initial reactor power levels due to the increased time to reach the SCRAM setpoint. The model parameters where the same as those described above, with the following exceptions: 1) the reactivity insertion was modeled as a linear ramp at a reactivity addition rate of $0.20/s, 2) a reactor scram was initiated 6.825 s after the initiation of the uncontrolled rod withdrawal (this corresponds to the time at which power reaches 300 kW plus an additional second to account for control rod insertion time), and 3) the rod experiencing the uncontrolled withdrawal was assumed to not SCRAM and continue its withdrawal. Strictly speaking, the latter of these exceptions assumes the simultaneous failure of the rod control circuit for the affected rod as well as the magnet which couples the rod to the control rod drive. Hence, continuing the rod withdrawal following the SCRAM will produce conservative results for this analysis due to the continued reactivity insertion of the rod experiencing the uncontrolled withdrawal. An additional measure of conservatism in this analysis is the use of a constant reactivity insertion rate of $0.20/s. In reality, the differential rod worth curve for the affected rod will have its largest value near the center of the core and will decrease as the rod approaches the end of its travel, as such the reactivity insertion rate will decrease as the transient proceeds. For the transient described above, the peak power was 10.3 MW, producing

a core average fuel temperature increase of 72.15 °C. Using a peaking factor of 2.613, this results in a maximum temperature in the highest power rod of 213.5 °C which is well below the DTRR fuel temperature Safety Limit of 500 °C. Even with the several layers of conservatism built into the present analysis, there is ample margin to the Safety Limit.

4. Summary

A detailed analysis of the thermal hydraulic analysis of the DTRR has been performed using RELAP5-3D in conjunction with information from the recent neutronics analysis of the DTRR using MCNP5. The analysis demonstrates that natural circulation cooling provides adequate cooling of the DTRR core under all operating conditions. The minimum DNBR (based upon the Bernath correlation) for the current DTRR core was 6.81 under the most limiting thermal hydraulic conditions which are permitted by the DTRR Technical Specifications. The minimum DNBR for a hypothetical arrangement of the DTRR core which results in exaggerated power peaking (denoted as the LCC in the neutronics report) was 6.74 (based upon the Bernath correlation).

Reactivity transients corresponding to 1) the step insertion of the maximum reactivity worth of a moveable experiment ($0.75) and 2) the uncontrolled withdrawal of a control rod at the maximum reactivity insertion rate ($0.20/s) were both simulated. The step insertion of reactivity was determined to be the bounding transient, which when initiated from the maximum licensed power level for the DTRR of 300 kW, resulted in a peak fuel temperature of 390.4 °C in the highest power rod. The uncontrolled rod withdrawal resulted in a peak temperature in the highest power rod of 213.5 °C. Both of these results are well below the DTRR fuel temperature Safety Limit of 500 °C, and as such they confirm the adequacy of the current DTRR licensing basis.

ANALYSIS OF THE NEUTRONIC BEHAVIOR

OF THE

DOW TRIGA RESEARCH REACTOR

Submitted to the NRC in support of the DTRR License Renewal

Prepared by:

Michael R Hartman

03 December 2011

TABLE OF CONTENTS

LIST OF TABLES

LIST OF FIGURES

1. Introduction

The following report summarizes an investigation into the neutronic behavior of the DOW TRIGA Research Reactor (DTRR). The DTRR is a TRIGA Mark-I reactor which is licensed to operate at powers up to 300 kW. The reactor consists of a series of six concentric rings in which are located fuel elements, graphite reflectors, and various experimental facilities. The core is surrounded by a cylindrical annulus of graphite which acts as a neutron reflector. The core and reflector are located in a below-grade aluminum tank filled with high-purity water. The water acts as a neutron moderator, a coolant, and as a radiation shield.

The purpose of this report is to provide a modern analysis of the neutronic characteristics of the DTRR in support of a 20-year license renewal through the U.S. Nuclear Regulatory Commission. Modeling of the DTRR was done using MCNP5[1], a general purpose Monte-Carlo code which is capable of high-fidelity modeling of the DTRR. The results of the MCNP5 modeling provide a basis to evaluate the neutronic performance of the DTRR in support of the license renewal.

2. Core Model

The MCNP5 model was constructed using facility drawings and technical data acquired from General Atomics (GA). Representative views of the MCNP5 model are shown in Figures 1,2, and 3.

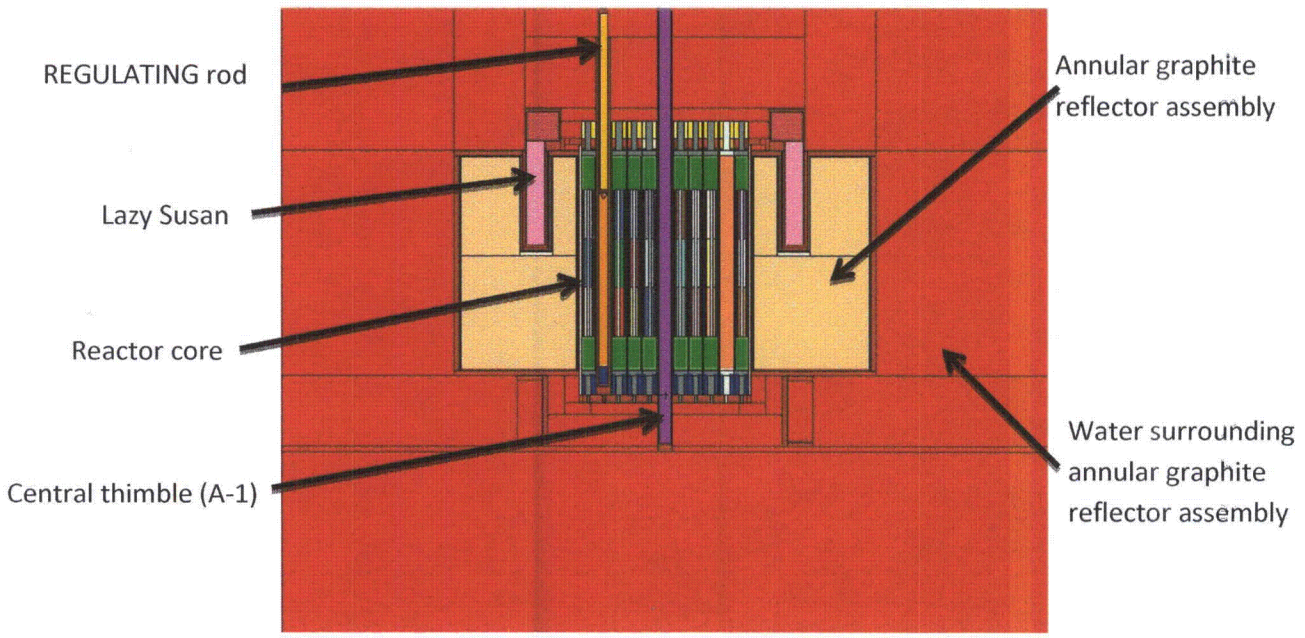

Figure 1. Vertical cross section of the MCNP5 model developed for the DTRR.

1. "MCNP – A General Monte Carlo N-Particle Code, Version 5," LA-CP-03-0245, F. B. Brown, Ed., Los Alamos National Laboratory (2003).

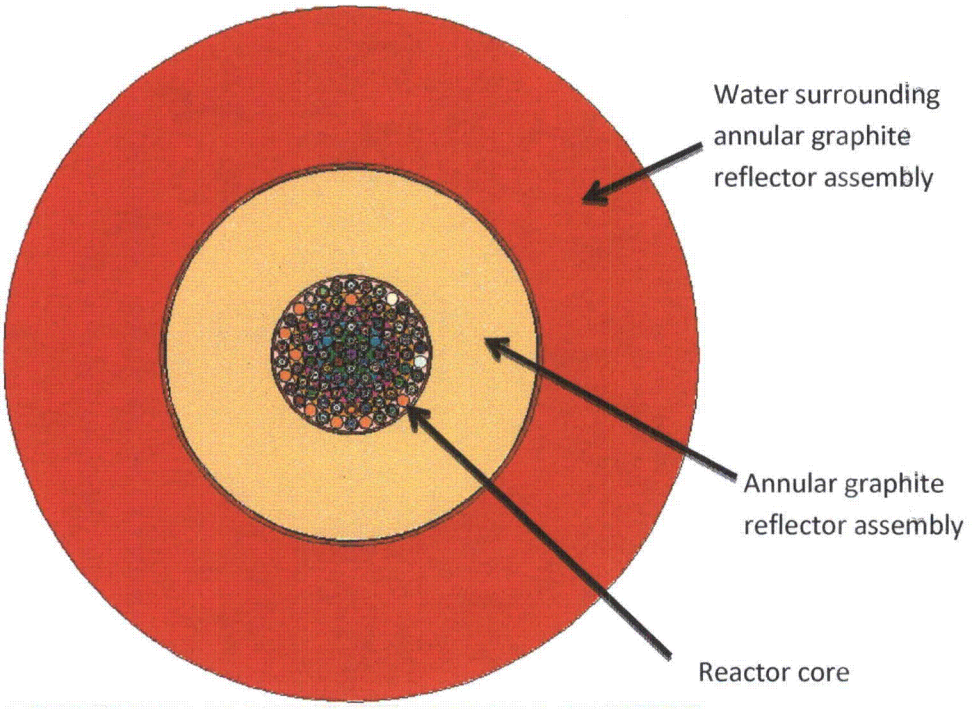

Figure 2. Horizontal cross section of the MCNP5 model developed for the DTRR taken at the mid-plane of the active fuel region.

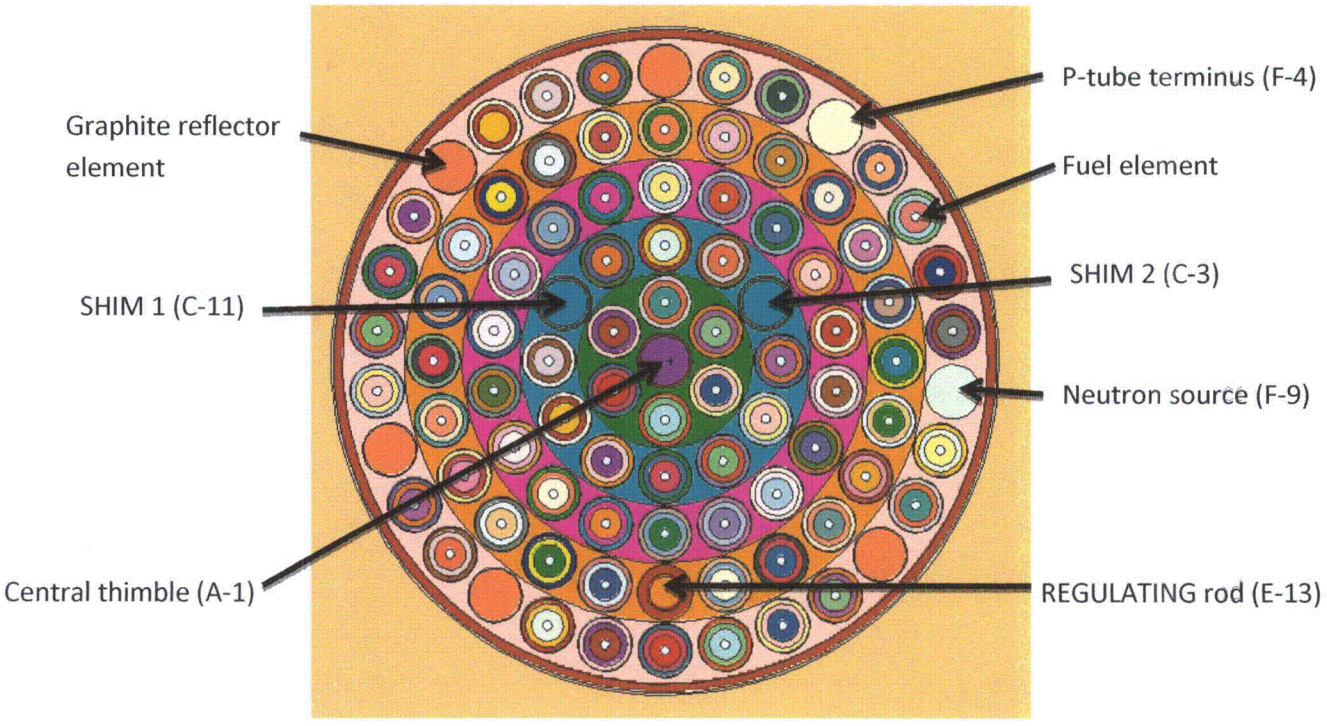

Figure 3. Horizontal cross section of the MCNP5 model developed for the DTRR taken at the mid-plane of the active fuel region, demonstrating the details of the model within the reactor core region. Grid locations for select locations are shown in parentheses. (2011 core configuration)

Historically, the arrangement of fuel and experimental facilities within the DTRR has consisted of essentially six different configurations. The detailed location-by-location arrangement of these configurations is provided in Appendix A. The first of these arrangements, shown in Figure 4, corresponds to the initial core configuration which was attained when the DTRR was first taken critical on 06 July 1967. The fuel for this initial core loading consisted of stainless steel-clad used fuel elements which were purchased from GA. Following the initial criticality, more fuel elements, including a new aluminum-clad element, were added to increase the core excess reactivity. Following the addition of this additional fuel, the DTRR core assumed a configuration similar to that which existed during the 1987 fuel inspection, shown in Figure 5. In 1991, two new stainless-steel clad fuel elements were introduced into the DTRR in grid locations F15 and F17, replacing the graphite reflector elements which had previously occupied these locations in the 1987 core configuration. The 1991 core arrangement is shown in Figure 6. In 1997, several elements within the B-ring and C-ring were interchanged, and additionally, the graphite elements in grid locations E1 and E19 were interchanged with the fuel elements in F1 and F29, respectively, resulting in the arrangement shown in Figure 7. In 2001, the new fuel elements which were introduced into grid location F15 and F17 in 1991 were exchanged with the fuel elements in B5 and B4, respectively. This fuel movement resulted in a core with the same fuel arrangement for the 2001 core as that shown in Figure 7 for the 1997 core. In 2005, graphite reflector elements in grid locations F25 and F29 were replaced with new stainless-steel clad fuel elements. The 2005 core configuration, shown in Figure 8, has remained unchanged and represents the current arrangement of the DTRR core.

The DTRR is fueled with Standard TRIGA fuel comprised of a matrix of ZrH_x ($x \sim 1.6$) containing 8.5 wt. % of uranium with a nominal enrichment of 20 wt. % U-235. The arrangement of a typical fuel element is shown in Figure 9. All but one of the fuel elements in the DTRR core have stainless steel cladding, while the remaining element (F-28) is clad with aluminum. One of the most important aspects of performing an accurate analysis of the neutronic performance of the DTRR is the determination of the fuel composition throughout the lifetime of the core. While the "as manufactured" data was available for the fuel received from GA for the DTRR, the fuel was used and detailed records of the burnup history were unavailable. To overcome this limitation, a MCNP5 model of the 1967 critical core was established using the as manufactured data for the initial fuel composition. The model was used to establish the average intra-rod power distribution for the nine fuel segments within each element. Using this intra-rod distribution, the U-235 of each fuel element was reduced until good agreement was achieved between the model and the as-measured core excess reactivity for the 1967 critical core configuration. It was determined that a U-235 depletion of 10.55% for each element resulted in a MCNP5 model with a core excess of $0.21 which is to be compared with the 1967 critical core which had a measured core excess of $0.13. After establishing the initial U-235 content of each fuel element in the 1967 core, the various core arrangements and the recorded energy produced in these arrangements,

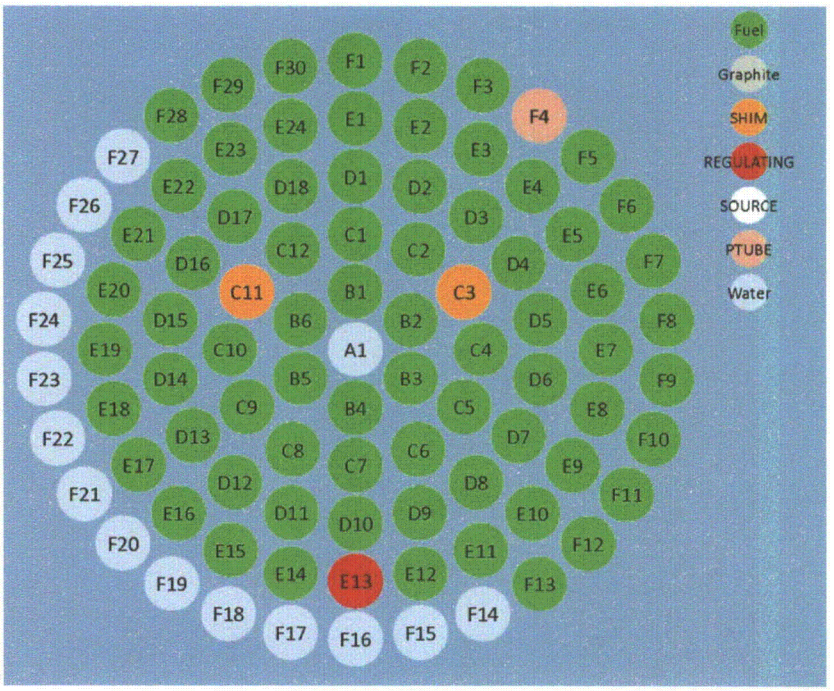

Figure 4. DTRR core configuration for the 1967 critical core. (72 fuel elements)

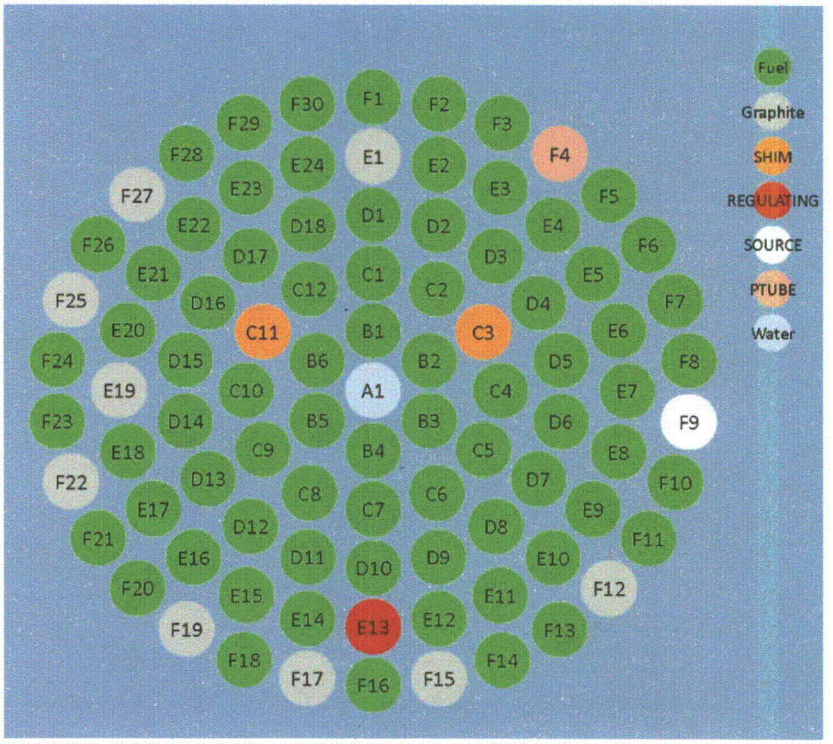

Figure 5. DTRR core configuration in 1987. This core arrangement served as the reference core for the period 1967-1991. (76 fuel elements)

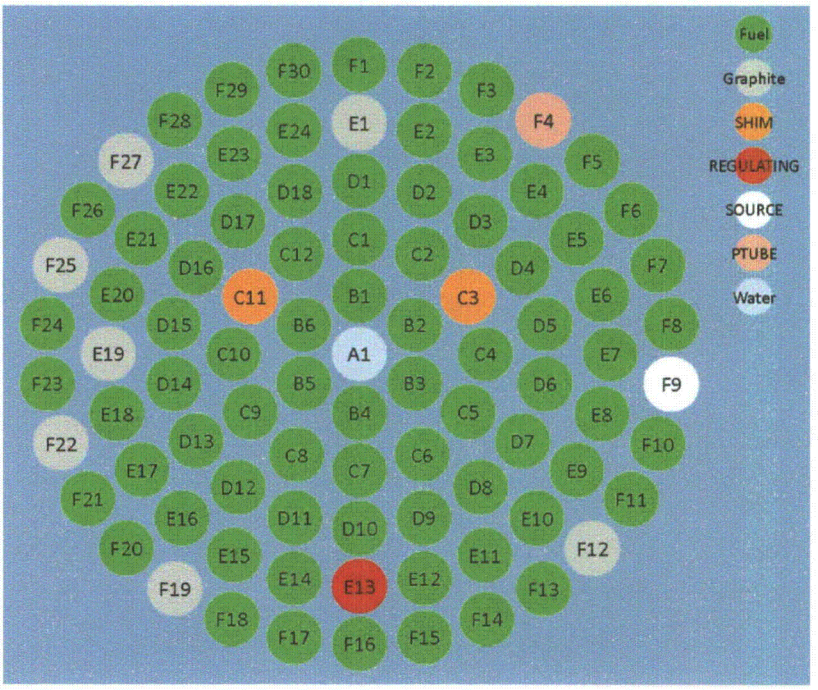

Figure 6. DTRR core configuration following the addition of fuel to grid locations F15 and F17 in 1991. (78 fuel elements)

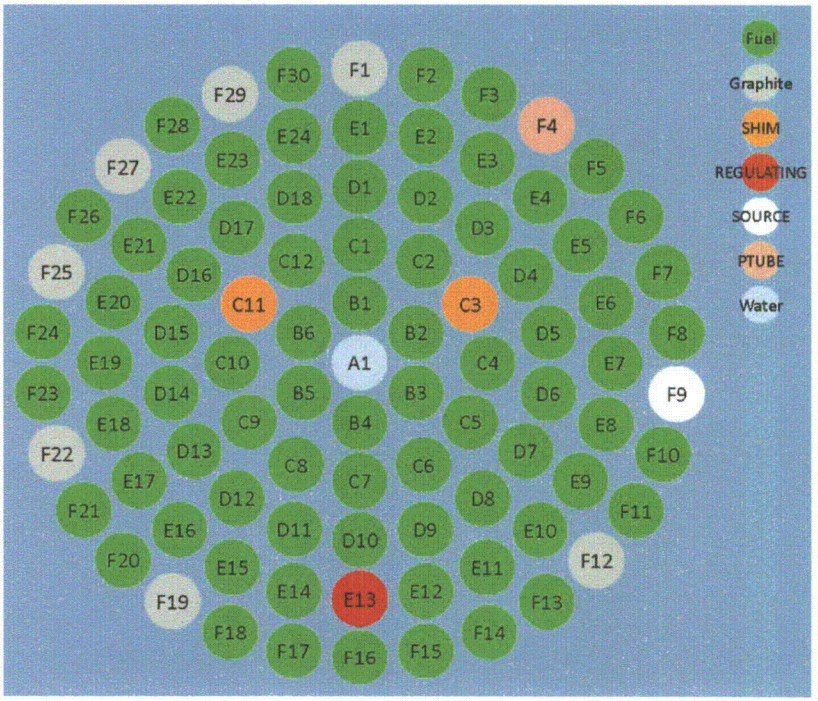

Figure 7. DTRR core configuration originally established in 1997. This core arrangement was retained following a fuel shuffle in 2001. (78 fuel elements)

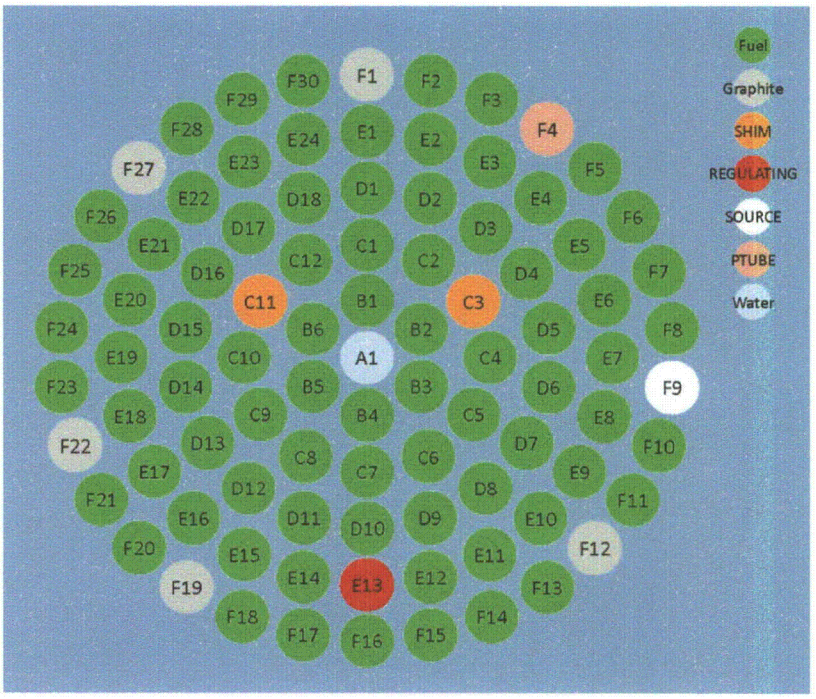

Figure 8. DTRR core arrangement in 2005 following the addition of fuel to grid locations F25 and F29. This core configuration represents the current core configuration. (80 fuel elements)

as detailed in Table 1,was used to deplete the U-235 content of each fuel segment within each element and determine the current value for use in the 2011 MCNP5 model. The material compositions used for other components within the DTRR MCNP5 model are listed in Table 2.

Table 1. Burnup history for various DTRR core configurations.

Burnup Segment	Energy produced [MWd]
1967 to 1991	9.60
1991 to 1997	8.51
1997 to 2001	6.59
2001 to 2005	6.94
2005 to 2011	8.70

Note: The arrangement shown is for a stainless steel clad element with a cladding thickness of 0.020". For an aluminum clad element, there is no zirconium pin and the cladding thickness is 0.030".

Figure 9. Schematic illustration of a standard TRIGA fuel element (left). The cross sectional view (right) displays the internal structure of the fuel element. Note that each of the individual fuel slugs was divided into three radial segments within the MCNP5 model to permit the determination of intra-rod power distributions and uranium depletion.

Table 2. Material composition for core components within the MCNP5 model of the DTRR core.

Material	Physical Density [g/cm3]	Element	Mass Fraction [g/g]
Type 304 Stainless Steel	7.857	C Mn Si P S Cr Ni Fe	3.500E-04 1.000E-02 5.000E-03 2.500E-04 1.000E-04 1.850E-01 9.250E-02 7.068E-01
Graphite Reflector in fuel element	1.560	C	1.000
Graphite in Graphite Reflector Elements	1.620	C	1.000
Graphite in Annular Reflector Assembly	1.75	C	1.000
Zirconium Fuel Pin	6.506	Zr	1.000
Aluminum 1100	2.700	Al B	1.000 1.000E-06
Aluminum 6061-T6	2.700	Si Fe Cu Mn Mg Cr Zn B Al	6.000E-03 3.500E-03 2.800E-03 7.000E-04 1.000E-02 2.000E-03 1.291E-03 1.000E-06 9.7373E-01
Water	1.000	H O	1.119E-01 8.881E-01
Air	1.029E-03	N O	0.800 0.200
Stainless Steel + Water Mix for Triflute Region (all elements except B4, B5, F25, and F29 in the 2011 Core Arrangement)	4.429	C Mn Si P S Cr Ni Fe H O	3.105E-04 8.871E-03 4.435E-03 2.218E-04 8.871E-05 1.641E-01 8.206E-02 6.270E-01 1.263E-02 1.003E-01
Stainless Steel + Water Mix for Triflute Region (elements B4, B5, F25, and F29 in the 2011 Core Arrangement)	3.262	C Mn Si P S Cr Ni Fe H O	2.781E-04 7.947E-03 3.973E-03 1.987E-04 7.947E-05 1.470E-01 7.351E-02 5.617E-01 2.297E-02 1.824E-01

Material	Physical Density [g/cm3]	Element	Mass Fraction [g/g]
Stainless Steel + Air in Lazy Susan	7.867E-01	C	3.496E-04
		Mn	9.988E-03
		Si	4.994E-03
		P	2.497E-04
		S	9.988E-05
		Cr	1.848E-01
		Ni	9.239E-02
		Fe	7.060E-01
		N	9.418E-04
		O	2.355E-04
Aluminum + Air in Lazy Susan	2.709E-01	Si	5.979E-03
		Fe	3.488E-03
		Cu	2.790E-03
		Mn	6.976E-04
		Mg	9.966E-03
		Cr	1.993E-03
		Zn	1.287E-03
		B	9.966E-07
		Al	9.704E-01
		N	2.735E-03
		O	6.837E-04
Boron Carbide in Control Rods	1.764	B	7.826E-01
		C	2.174E-01
Aluminum + Water for Triflute Region of Graphite Reflector Elements and Aluminum-Clad Fuel	1.850	Si	4.378E-03
		Fe	2.554E-03
		Cu	2.043E-03
		Mn	5.108E-04
		Mg	7.297E-03
		Cr	1.459E-03
		Zn	9.422E-04
		B	7.297E-07
		Al	7.105E-01
		H	3.024E-02
		O	2.400E-01

3. Model Results

3.1 Effective Delayed Neutron Fraction

The effective delayed neutron fraction for the MCNP5 model representing the 2011 core configuration was determined using the expression

$$\beta_{eff} = 1 - \frac{k_p}{k_{p+d}},$$

where k_p is the system eigenvalue assuming all neutrons from fission are born with the energy distribution appropriate for prompt neutrons and k_{p+d} is the system eigenvalue where fission neutrons are born with an appropriately weighted energy distribution for both prompt and delayed neutrons. The effective delayed neutron fraction was determined to by 0.0070 $\pm$ 0.0003. This is identical to the value given in the DTRR Safety Analysis Report.

3.2 Control Rod Worth

The SHIM 1, SHIM 2, and REGULATING rods were calibrated using the rod positions from the actual rod calibration performed in January of 2011. Calibrating the rods in this manner is beneficial in that it permits the rod worths calculated using MCNP5 to be directly compared with experimental data, and in addition, it provides a number of critical rod configurations for the DTRR which can be utilized to assess the validity of the DTRR MCNP5 model for the 2011 core. MCNP5 simulations were performed to simulate the DTRR rod calibration procedure. The fourteen critical core configurations, detailed in Table 3, were used to determine how well the model predicts criticality for these rod positions. The results showed that criticality for these positions were predicted within less than 1% of the expected values. This implies that the MCNP5 model for the 2011 DTRR core provides a very good representation of the actual 2011 core. The rod pull simulations were used to determine the reactivity associated with each rod pull, and these were summed to determine the integral rod worth for each control rod. Note that due to the lower worth of the REGULATING rod, it is only possible to determine a portion of the integral rod worth curve for the SHIM 1 and SHIM 2 rods. The remainder of the integral rod worth curve for each rod is determined by fitting a curve to the data and extrapolating it over the uncalibrated portion of the rod. Initial comparison of the measured data from January of 2011 and the MCNP5 calculated values showed higher differences between the two data sets than expected. Through further investigation, it was discovered that the physical constants used in the In Hour equation to convert the measured reactor period to reactivity insertion for the January 2011 measured data were different from the presently accepted values. The measured data were reanalyzed using appropriate physical constants. After the correction to the measured data, the measured and calculated data were fitted using a similar procedure, and the agreement between the measured data and that generated using MCNP5 was found to be within 11.0%, 7.46%, and 4.17% for the SHIM 1, SHIM 2, and REGULATING rods, respectively. The results of the rod calibrations are shown in Figures 10, 11, and 12, and the integral rod worth for each rod is compared with the experimentally determined value in Table 4.

As an additional test of the MCNP5 model which was developed for the DTRR, the model was used to simulate the rod calibration performed in December of 1997. The core arrangement for the DTRR during this period of time is shown in Figure 7, and the details of the individual grid locations are provided in Appendix A. The 1997 rod calibration data contain seventeen critical cases which can be used to assess the ability of the MCNP5 model to predict criticality for drastically different control rod configurations. The seventeen critical core configurations, detailed in Table B1, were used to determine how well the model predicts criticality for these rod positions. The results show, once again, that criticality for these positions was predicted within less than 1% of the expected values. The resulting integral control rod worth curves for the SHIM 1, SHIM 2, and REGULATING rods are presented in Figures B1, B2, and B3 of Appendix B. The integral control rod curves show very good agreement between the measured and calculated data. Note that as compared with the MCNP5 simulations for the 2011 core, the calculated errors in the 1997 cases are larger. This is due primarily to statistical effects since

only shorter MCNP5 runs were performed for this analysis. Also note that it was necessary to correct the 1997 measured data using a process identical to that described above for the 2011 measured data.

Table 3: Rod positions from the January 2011 control rod calibration and the results of the corresponding MCNP5 simulations. The positions for the SHIM 1, SHIM 2, and REGULATING rods correspond to the measured data and were used explicitly in the MCNP5 calculations. The fourteen critical cases, labeled as "RC**x**c" are highlighted in green while the cases corresponding to the rod pulls are labeled as "RC**x**p", where **x** corresponds to the condition number in the test. The stated error in the MCNP5 results are $\pm$ 1 σ.

	Rod Position [steps]			MCNP5 RESULTS:	
Condition	Shim 1	Shim 2	Regulating	k_eff	σ_keff
RC1c	982	246	988	1.00084	0.00026
RC1p	982	311	988	1.00294	0.00024
RC2c	982	311	675	1.00015	0.00026
RC2p	982	391	675	1.0025	0.00027
RC3c	982	391	517	1.00052	0.00027
RC3p	982	449	517	1.00224	0.00026
RC4c	982	449	361	1.00063	0.00025
RC4p	982	514	361	1.00268	0.00027
RC5c	982	514	48	1.00016	0.00027
RC5p	982	584	48	1.00253	0.00027
RC6c	797	584	48	0.99947	0.00028
RC6p	797	661	48	1.00279	0.00027
RC7c	698	661	48	1.00011	0.00027
RC7p	698	735	48	1.00211	0.00026
RC8c	632	735	48	0.99971	0.00027
RC8p	632	807	48	1.00192	0.00023
RC9c	588	807	48	1.00004	0.00026
RC9p	588	992	48	1.00266	0.00025
RC10c	528	992	48	1.00016	0.00026
RC10p	528	992	339	1.00225	0.00027
RC11c	472	992	339	1.00035	0.00024
RC11p	472	992	491	1.00294	0.00027
RC12c	421	992	491	1.00019	0.00024
RC12p	421	992	639	1.00266	0.00026
RC13c	353	992	639	1.00042	0.00026
RC13p	353	992	988	1.00256	0.00026
RC14c	268	992	988	1.0007	0.00026

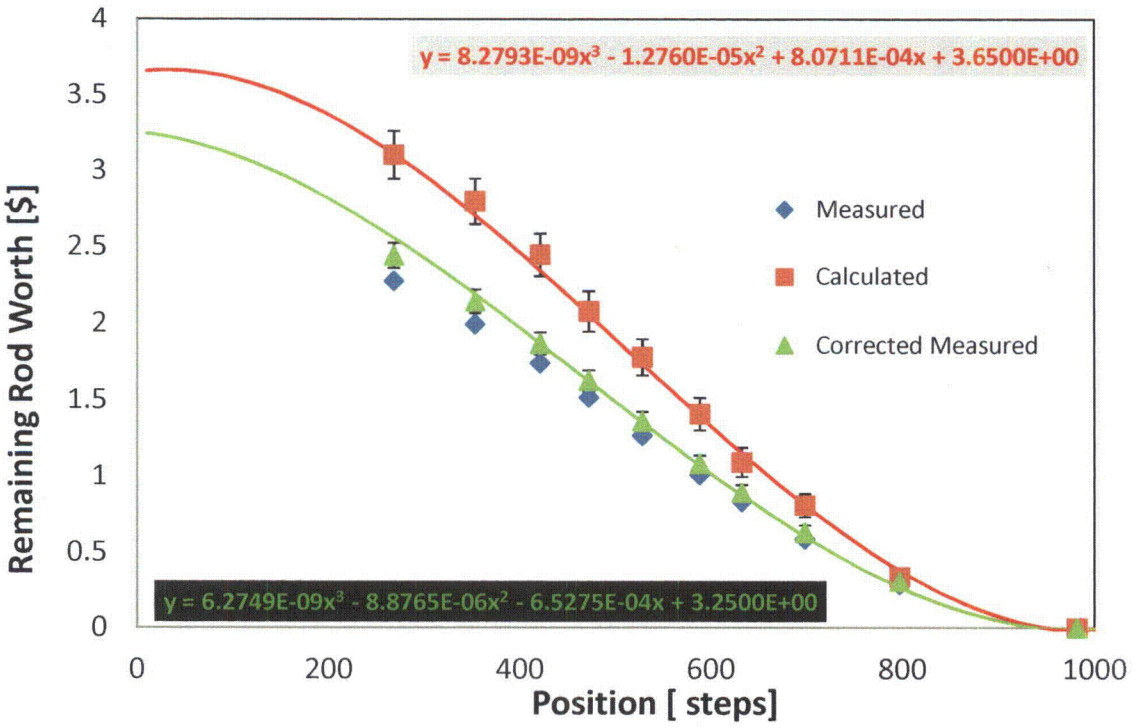

Figure 10. Integral rod worth curve for the SHIM 1 rod based on rod positions from the January 2011 DTRR rod calibration procedure.

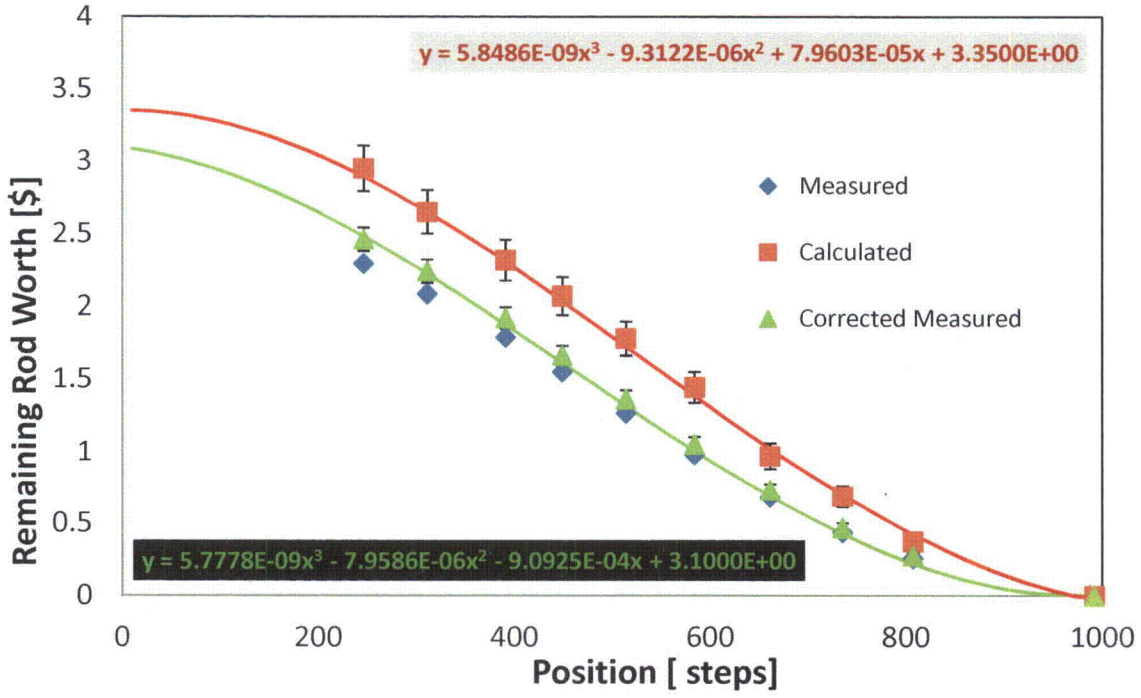

Figure 11. Integral rod worth curve for the SHIM 2 rod based on rod positions from the January 2011 DTRR rod calibration procedure.

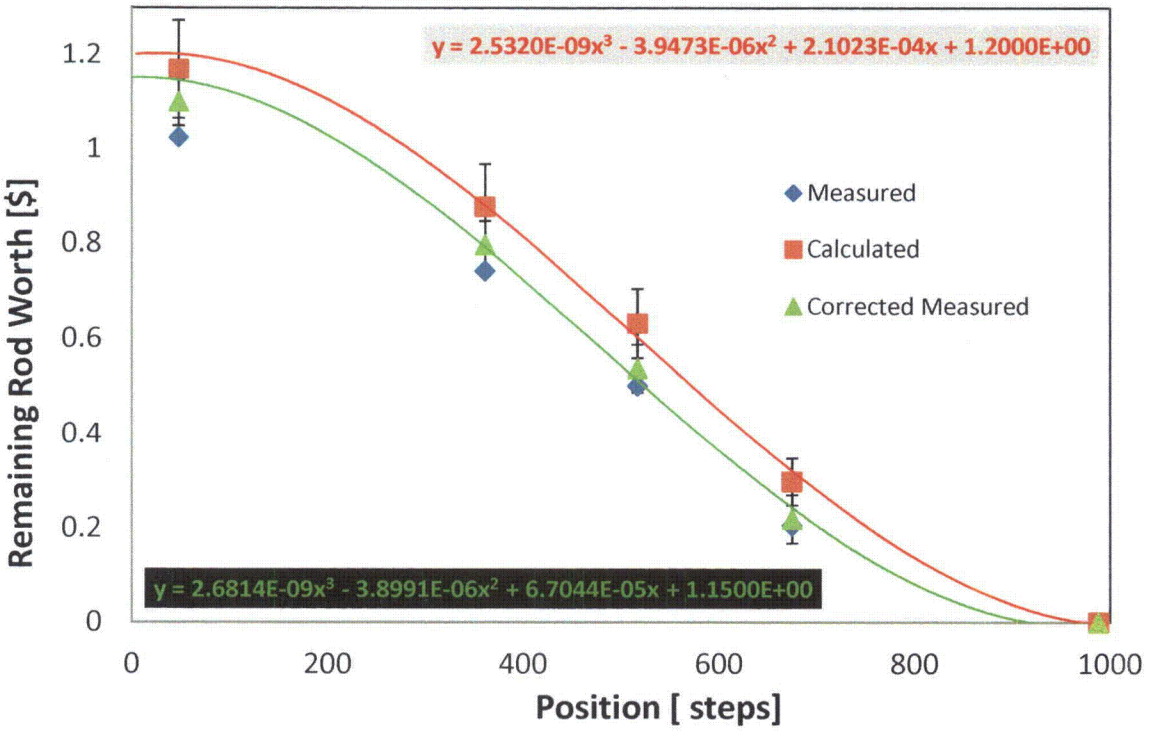

Figure 12. Integral rod worth curve for the REGULATING rod based on rod positions from the January 2011 DTRR rod calibration procedure

Table 4. Summary of integral control rod worths.

Control Rod	Corrected Measured Integral Rod Worth [$] from January 2011	MCNP5 Calculated Integral Rod Worth [$]	Difference [%] (Calc-Meas)/Calc*100
REGULATING	1.15	1.20 ± 0.11	4.17
SHIM 1	3.25	3.65 ± 0.16	11.0
SHIM 2	3.10	3.35 ± 0.16	7.46
Sum of all rods	7.50	8.20 ± 0.25	8.54

3.3 Shutdown Margin

The shutdown margin for the current DTRR core was determined using the MCNP5 calculated integral rod worths, listed in Table 3, in conjunction with the MCNP5 calculated core excess reactivity of $2.81 ± 0.04. The calculated shutdown margin was found using the relationship,

$$\text{Shutdown Margin} = \text{Total worth of all rods} - \text{Worth of most reactive rod} - \text{Core excess reactivity}$$

This is the same methodology utilized by the DTRR to calculate shutdown margin, based upon measured control rod worths. For the current core, the MCNP5 based shutdown margin was determined assuming that the SHIM 1 rod was fully withdrawn from the core, yielding a shutdown margin of \$1.74 $\pm$ 0.30. The calculated shutdown margin exceeded the minimum shutdown margin of \$0.50 specified within the DTRR Technical Specifications for all core conditions.

3.4 Fuel Prompt-Temperature Coefficient

The prompt-temperature coefficient for the DTRR, α_f, was calculated by varying the fuel temperature within the MCNP5 model along with the thermal neutron libraries, $S(\alpha,\beta)$, for the hydrogen and zirconium within the zirconium hydride matrix which contains the fuel. Due to the limited cross section libraries available within MCNP5, simulations could only be performed at a limited number of temperatures. Calculations were performed at 293.6 K, 600 K, 900 K, and 1200 K. There are no $S(\alpha,\beta)$ libraries for zirconium and hydrogen at 900 K, so the 900 K data point was obtained by simulating the fuel temperature at 900 K through the proper choice of cross section libraries for the isotopes found within the fuel, and then performing two simulations using $S(\alpha,\beta)$ data at 800 K and 1000 K. The MCNP5 simulation results corresponding to $S(\alpha,\beta)$ at 800 K and 1000 K were then arithmetically averaged to determine an appropriate value at 900 K. The results of this calculation are shown in Figure 13 and summarized in Table 5 below.

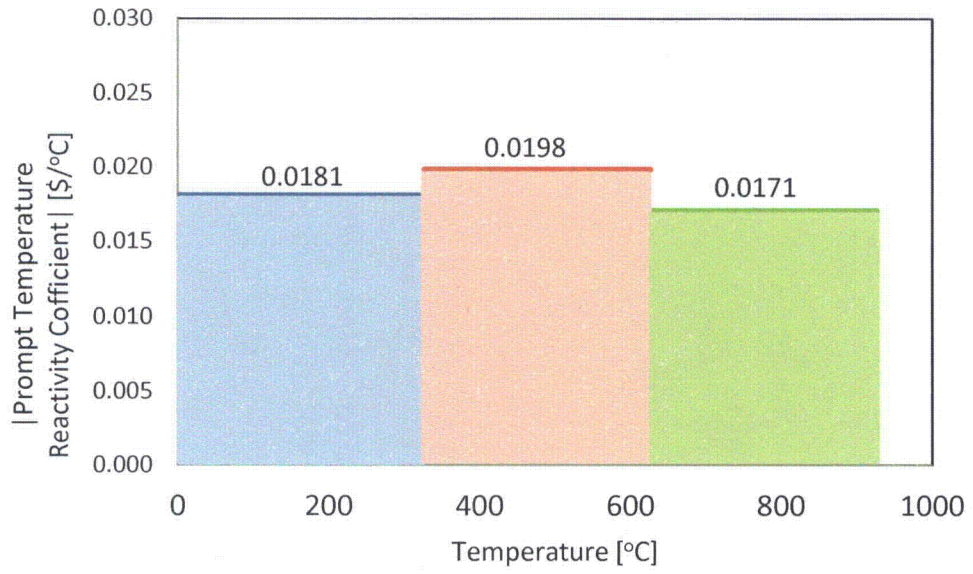

Figure 13. Results of the MCNP5 calculation of the prompt-temperature coefficient for the DTRR fuel. The magnitude of the prompt-temperature coefficient is shown as a function of temperature with the average value over a temperature region shown above that region.

Table 5. Summary of MCNP5 prompt-temperature coefficient calculations.

Temperature Range [°C]	Fuel Prompt-Temperature Coefficient [$/°C]
0 to 327	-0.0181
327 to 627	-0.0198
627 to 927	-0.0171

3.5 Core Power Distribution

Using the MCNP5 model, the core power distribution for the 2011 core configuration was found for an operating power of 300 kW with all rods fully withdrawn from the core. The power produced in each element is shown in Figure 14. The average element power was determined to be 3.75 kW while the element which produced the maximum power was found to be in grid location B-6, producing 5.91 kW.

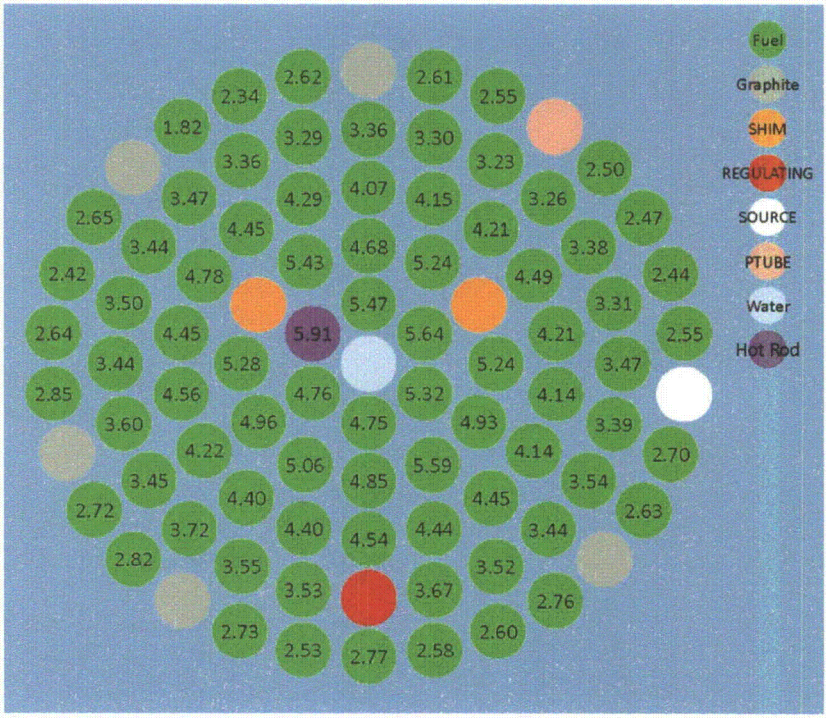

Figure 14. Map of the DTRR core showing the power per element at the maximum allowable operating power of 300 kW for the 2011 core configuration. The hot rod is found to be in location B-6 with an element power of 5.91 kW. (80 fuel elements)

3.6 Limiting Core Configuration

In an effort to determine the maximum power per element which could be expected for the DTRR core, a hypothetical core, denoted as the limiting core configuration (LCC), was modeled using MCNP5. In the LCC, the fuel in the B-ring was replaced with fresh fuel which had the

nominal composition of the fuel added to the core in 2005. This fuel was chosen to be representative of fuel which would be manufactured under current fuel specifications and modern fabrication techniques. In addition to the replacement of the burnt fuel in the B-ring with fresh fuel, four low-power elements on the periphery of the core were replaced with graphite reflector elements. The model was again run with all rods completely withdrawn from the core. The calculated core excess for the LCC was \$2.24 $\pm$ 0.06. The average element power was determined to be 3.95 kW while the element which produced the maximum power was found to be in grid location C-6, producing 6.08 kW. The LCC represents an extreme modification of the current 2011 core configuration, and while the hot rod was found to produce more power in the LCC, it was only ~3% higher than in the current 2011 core configuration. The LCC and the power per element at a core power of 300 kW are shown in Figure 15. Additional calculations to determine the integral control rod worth curves for the LCC were not necessary because the integral rod worth curves presented earlier are adequate since the power profiles in the LCC and the 2011 core are similar.

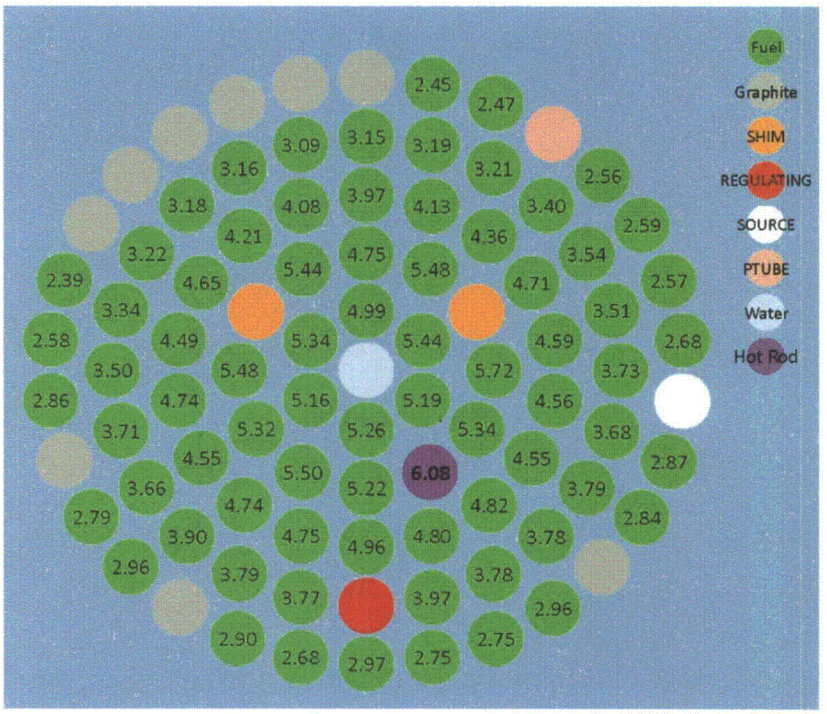

Figure 15. Map of the DTRR core showing the power per element at the maximum allowable operating power of 300 kW for the limiting core configuration. The hot rod is found to be in location C-6 with an element power of 6.08 kW. (76 fuel elements)

4. Summary

The DTRR was simulated using MCNP5 to determine select core physics parameters such as beta-effective (β_{eff}), integral control rod worth, shutdown margin, and the fuel prompt-temperature reactivity coefficient (α_f). The results of this analysis demonstrate that the licensing basis established in the DTRR Technical Specifications is valid, and furthermore that the reactor physics parameters used in various safety analyses within the DTRR Safety Analysis Report are in reasonable agreement with the values calculated herein.

APPENDIX A

SUMMARY OF DTRR CORE LOADING CONFIGURATIONS UTILIZED IN THE ANALYSIS OF THE NETURON BEHAVIOR

Table A1. The table below summarizes the core loading for the core configurations utilized within this analysis. Grid locations shaded in green represent a change in the loading of that particular location relative to the prior core configuration. The yellow shading for grid location F28 indicates the presence of an aluminum clad element in that location.

	Element Identification						
	Year						
Grid Location	1967	1987	1991	1997	2001	2005	2011
A1	****	****	****	****	****	****	****
B1	4099	4099	4099	2402	2402	2402	2402
B2	4100	4100	4100	4076	4076	4076	4076
B3	4115	4115	4115	4115	4115	4115	4115
B4	4093	4093	4093	4100	10220	10220	10220
B5	4116	4116	4116	4059	10219	10219	10219
B6	4059	4059	4059	2437	2437	2437	2437
C1	4076	4076	4076	4093	4093	4093	4093
C2	2426	2426	2426	2426	2426	2426	2426
C3	SHIM 2	SHIM 2	SHIM 2	SHIM 2	SHIM 2	SHIM 2	SHIM 2
C4	2363	2363	2363	2363	2363	2363	2363
C5	2433	2433	2433	2433	2433	2433	2433
C6	2424	2424	2424	2424	2424	2424	2424
C7	2402	2402	2402	4099	4099	4099	4099
C8	2437	2437	2437	2442	2442	2442	2442
C9	2454	2454	2454	2454	2454	2454	2454
C10	2364	2364	2364	4116	4116	4116	4116
C11	SHIM 1	SHIM 1	SHIM 1	SHIM 1	SHIM 1	SHIM 1	SHIM 1
C12	2442	2442	2442	2364	2364	2364	2364
D1	2398	2398	2398	2398	2398	2398	2398
D2	2384	2384	2384	2384	2384	2384	2384
D3	2395	2395	2395	2395	2395	2395	2395
D4	2378	2378	2378	2378	2378	2378	2378
D5	2381	2381	2381	2381	2381	2381	2381
D6	2396	2396	2396	2396	2396	2396	2396
D7	2370	2370	2370	2370	2370	2370	2370
D8	2440	2440	2440	2440	2440	2440	2440
D9	2432	2432	2432	2432	2432	2432	2432
D10	2434	2434	2434	2434	2434	2434	2434
D11	2455	2455	2455	2455	2455	2455	2455
D12	2453	2453	2453	2453	2453	2453	2453
D13	2438	2438	2438	2438	2438	2438	2438
D14	2421	2421	2421	2421	2421	2421	2421
D15	2429	2429	2429	2429	2429	2429	2429
D16	2365	2365	2365	2365	2365	2365	2365

D17	2408	2408	2408	2408	2408	2408	2408
D18	2449	2499	2499	2449	2449	2449	2449
E1	2428	GRAPHITE	GRAPHITE	4092	4092	4092	4092
E2	2367	2367	2367	2367	2367	2367	2367
E3	2399	2399	2399	2399	2399	2399	2399
E4	2415	2415	2415	2415	2415	2415	2415
E5	3398	3398	3398	3398	3398	3398	3398
E6	2416	2416	2416	2416	2416	2416	2416
E7	2403	2379	2379	2379	2379	2379	2379
E8	2392	2392	2392	2392	2392	2392	2392
E9	2423	2423	2423	2423	2423	2423	2423
E10	2431	2439	2439	2439	2439	2439	2439
E11	2412	2412	2412	2412	2412	2412	2412
E12	3021	3021	3021	3021	3021	3021	3021
E13	REGULATING	REGULATING	REGULATING	REGULATING	REGULATING	REGULATING	REGULATING
E14	2390	2390	2390	2390	2390	2390	2390
E15	2422	2422	2422	2422	2422	2422	2422
E16	3015	2386	2386	2386	2386	2386	2386
E17	2427	2427	2427	2427	2427	2427	2427
E18	2417	2417	2417	2417	2417	2417	2417
E19	3509	GRAPHITE	GRAPHITE	2380	2380	2380	2380
E20	4056	4056	4056	4056	4056	4056	4056
E21	4124	4124	4124	4124	4124	4124	4124
E22	3823	2428	2428	2428	2428	2428	2428
E23	3824	3824	3824	3824	3824	3824	3824
E24	3822	3822	3822	3822	3822	3822	3822
F1	4092	4092	4092	GRAPHITE	GRAPHITE	GRAPHITE	GRAPHITE
F2	4073	4073	4073	4073	4073	4073	4073
F3	4075	4075	4075	4075	4075	4075	4075
F4	RABBIT	RABBIT	RABBIT	RABBIT	RABBIT	RABBIT	RABBIT
F5	4112	4112	4112	4112	4112	4112	4112
F6	4101	4101	4101	4101	4101	4101	4101
F7	4052	4052	4052	4052	4052	4052	4052
F8	4067	4067	4067	4067	4067	4067	4067
F9	2379	SOURCE	SOURCE	SOURCE	SOURCE	SOURCE	SOURCE
F10	2372	2372	2372	2372	2372	2372	2372
F11	2444	2403	2403	2403	2403	2403	2403
F12	2441	GRAPHITE	GRAPHITE	GRAPHITE	GRAPHITE	GRAPHITE	GRAPHITE
F13	2420	2420	2420	2420	2420	2420	2420
F14	WATER	2441	2441	2441	2441	2441	2441
F15	WATER	GRAPHITE	10219	10219	4059	4059	4059
F16	WATER	2431	2431	2431	2431	2431	2431
F17	WATER	GRAPHITE	10220	10220	4100	4100	4100
F18	WATER	3015	3015	3015	3015	3015	3015
F19	WATER	GRAPHITE	GRAPHITE	GRAPHITE	GRAPHITE	GRAPHITE	GRAPHITE

F20	WATER	2393	2393	2393	2393	2393	2393
F21	WATER	2444	2444	2444	2444	2444	2444
F22	WATER	GRAPHITE	GRAPHITE	GRAPHITE	GRAPHITE	GRAPHITE	GRAPHITE
F23	WATER	2376	2376	2376	2376	2376	2376
F24	WATER	3509	3509	3509	3509	3509	3509
F25	WATER	GRAPHITE	GRAPHITE	GRAPHITE	GRAPHITE	11359	11359
F26	WATER	3823	3823	3823	3823	3823	3823
F27	WATER	GRAPHITE	GRAPHITE	GRAPHITE	GRAPHITE	GRAPHITE	GRAPHITE
F28	2397	4969	4969	4969	4969	4969	4969
F29	2380	2380	2380	GRAPHITE	GRAPHITE	11358	11358
F30	2409	2409	2409	2409	2409	2409	2409

APPENDIX B

SUMMARY OF DTRR CONTROL ROD CALIBRATION DATA FOR THE DECEMBER 1997 ROD CALIBRATION

Table B1. Rod positions from the December 1997 control rod calibration and the results of the corresponding MCNP5 simulations. The positions for the SHIM 1, SHIM 2, and REGULATING rods correspond to the measured data and were used explicitly in the MCNP5 calculations. The seventeen critical cases, labeled as "RC**x**c" are highlighted in green while the cases corresponding to the rod pulls are labeled as "RC**x**p", where **x** corresponds to the condition number in the test. The stated error in the MCNP5 results are $\pm$ 1 σ.

	Rod Position [steps]			MCNP RESULTS:	
Condition	Shim 1	Shim 2	Regulating	k_eff	σ_k
RC1c	992	306	987	0.99914	0.0004
RC1p	992	342	987	0.99917	0.00042
RC2c	992	342	757	0.99775	0.00041
RC2p	992	391	757	1	0.00042
RC3c	992	391	622	0.99875	0.0004
RC3p	992	438	622	0.99883	0.00042
RC4c	992	438	519	0.99705	0.00042
RC4p	992	487	519	0.99968	0.00041
RC5c	992	487	400	0.99747	0.00038
RC5p	992	541	400	0.99927	0.0004
RC6c	992	541	227	0.99797	0.0004
RC6p	992	577	227	0.99803	0.0004
RC7c	992	577	12	0.99822	0.00042
RC7p	992	630	12	1.0005	0.00039
RC8c	837	630	12	0.99791	0.00041
RC8p	837	689	12	0.99897	0.00039
RC9c	755	689	12	0.99808	0.00042
RC9p	755	760	12	0.99988	0.00041
RC10c	683	760	12	0.99779	0.00041
RC10p	683	833	12	0.99938	0.00041
RC11c	636	833	12	0.99908	0.00041
RC11p	636	991	12	0.99964	0.0004
RC12c	586	991	12	0.99849	0.0004
RC12p	586	991	296	0.99972	0.00038
RC13c	530	991	296	0.99866	0.00039
RC13p	530	991	449	1.00054	0.00042
RC14c	474	991	449	0.99743	0.00041
RC14p	474	991	597	1.00094	0.00039
RC15c	409	991	597	0.99864	0.00043
RC15p	409	991	727	0.9998	0.00043
RC16c	347	991	727	0.9996	0.0004
RC16p	347	991	987	1.00113	0.0004
RC17c	301	991	987	0.99892	0.00037

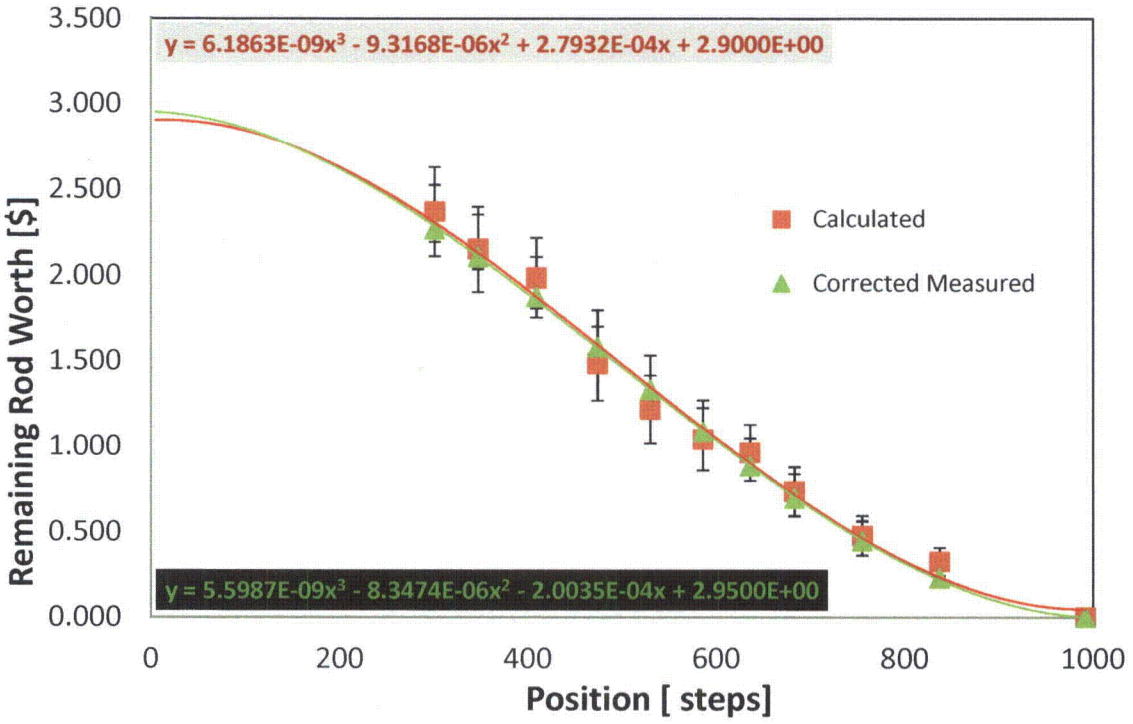

Figure B1. Integral rod worth curve for the SHIM 1 rod based on rod positions from the December 1997 DTRR rod calibration procedure.

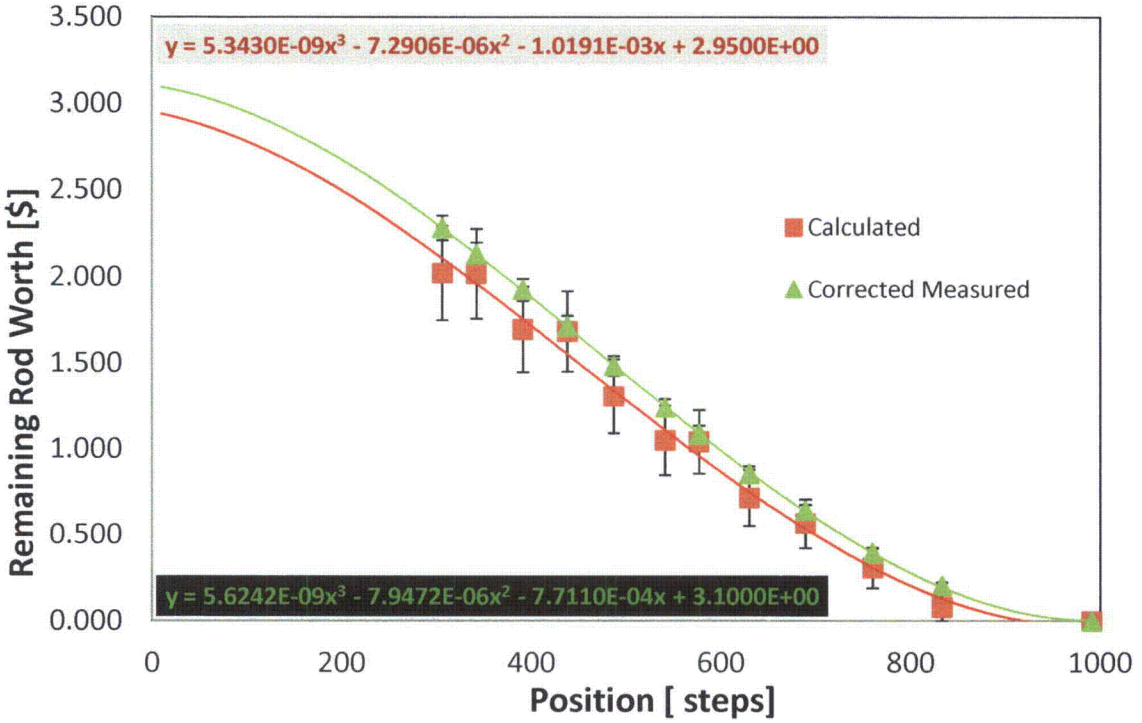

Figure B2. Integral rod worth curve for the SHIM 2 rod based on rod positions from the December 1997 DTRR rod calibration procedure.

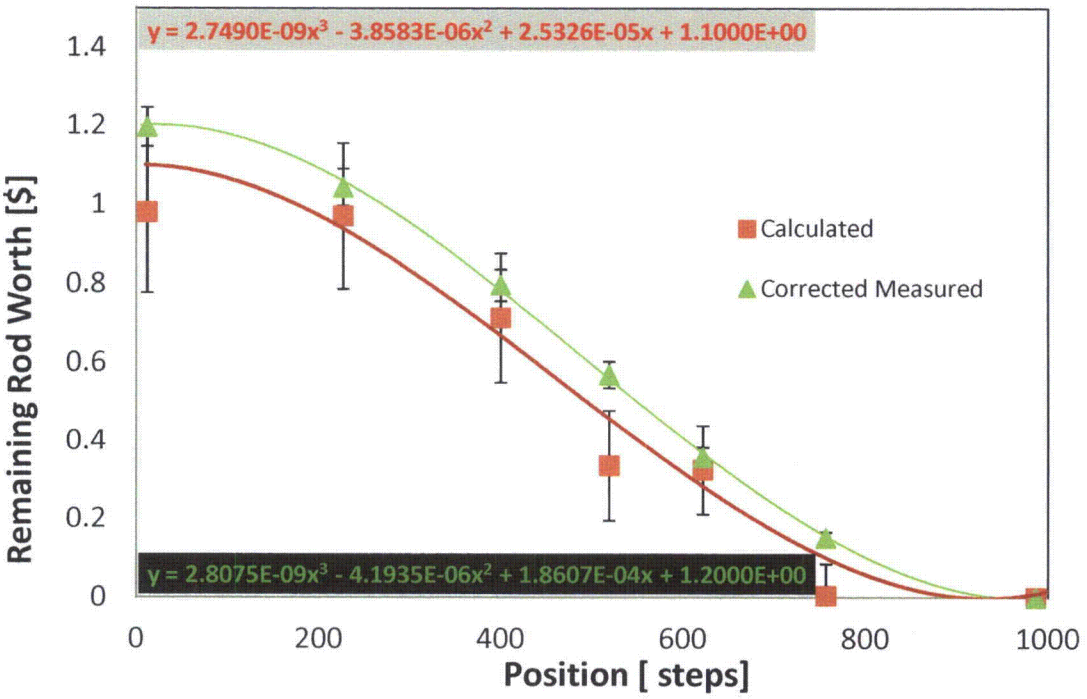

Figure B3. Integral rod worth curve for the REGULATING rod based on rod positions from the December 1997 DTRR rod calibration procedure.